Supplementary Information (SI) for Nanoscale Horizons.

Supporting Information

Hyperconjugated Linker Design in Gaint Dimeric Donors Enabled Superior Short-Circuit Current in Organic Solar Cells

Caixuan Wang[1,2], Mengying Wu[1,3], Dan Deng[1,*], Ruixiang Fang[1,4], Jianqi Zhang[1], Ruimin Zhou[3,*], Zhixiang Wei[1,2*]

[1]Key Laboratory of Nanosystem and Hierarchical Fabrication of Chinese Academy of Sciences, National Center for Nanoscience and Technology, Beijing 100190, China

[2]University of Chinese Academy of Sciences, Beijing 100049, China

[3]College of Chemistry, Zhengzhou University, Zhengzhou 450001, China

[4]Key Laboratory of Flexible Electronics & Institute of Advanced Materials, Nanjing Tech University, Jiangsu 211816, China

Correspondence: dengd@nanoctr.cn (D.D.), zhourm@zzu.edu.cn (R.M.Z.), weizx@nanoctr.cn (Z.X.W.)

Supplementary Methods

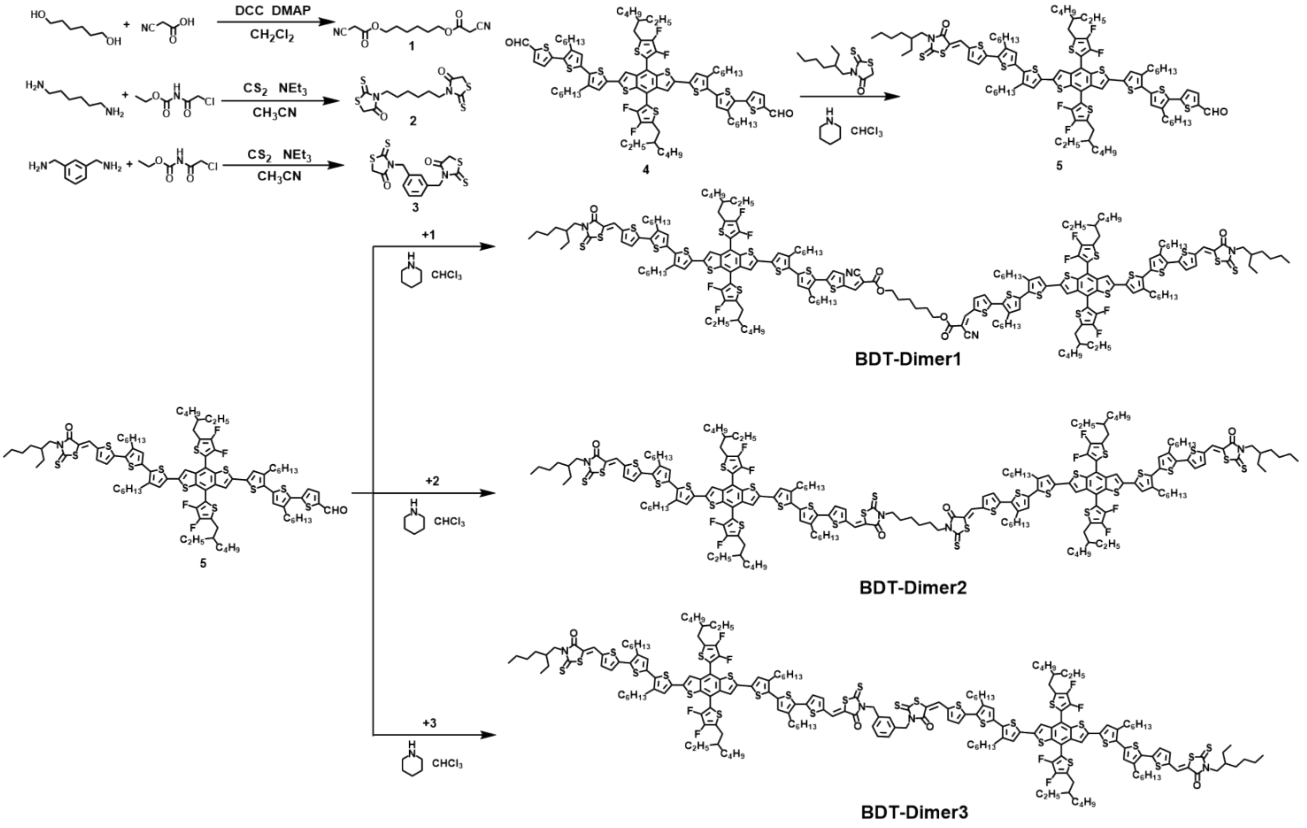

Scheme S1. Synthetic routes for BDT-Dimers.

Materials and Synthesis procedure

Compound 1. Dissolved 2-cyanoacetic acid (360 mg, 4.24 mmol) and hexane-1,6-diol (250 mg, 2.12 mmol) in dichloromethane, added N,N-dimethylpyridin-4-amine (25.8 mg, 0.21 mmol) to the solution and stirred for 5 minutes at room temperature. Dissolved (E)-1,2-dicyclohexyldiazene (1091 mg, 5.29 mmol) in dichloromethane, added it dropwise to the reaction solution and stirred for 6 hours. Filtered the solution and removed the solvent by rotary evaporation. The crude product was further purified by silica gel column chromatography (petroleum ether: DCM = 1:4) to afford compound 2 as light yellow solid. (430 mg, 80.6%). ^{1}H NMR (400 MHz, $CDCl_3$) δ = 4.22 (t, *J*=6.5, 4H), 3.46 (s, 4H), 1.74–1.66 (m, 4H), 1.45–1.38 (m, 4H).

Compound 2. Dissolved hexane-1,6-diamine (426 mg, 3.67 mmol) in acetonitrile, added triethylamine (1.22 mL, 8.81 mmol) to the solution and stirred for 5 minutes at room temperature. Dissolved ethyl

(2-chloroacetyl)carbamate (1216 mg, 7.34 mmol) in acetonitrile and added to the reaction solution, then CS_2 (0.44 mL, 7.34 mmol) was added and stirred for 30 minutes. The reaction mixture was poured into water and extracted with DCM three times. The crude product was further purified by silica gel column chromatography (petroleum ether: DCM = 1:2) to afford compound 1 as light yellow solid. (1128 mg, 88.3%). ^{1}H NMR (400 MHz, $CDCl_3$) δ = 4.48 (s, 4H), 3.97 (t, *J*=6.8, 4H), 1.68–1.59 (m, 4H), 1.39–1.29 (m, 4H).

Compound 3. Dissolved 1,3-phenylenedimethanamine (500 mg, 3.67 mmol) in acetonitrile, added triethylamine (1.22 mL, 8.81 mmol) to the solution and stirred for 5 minutes at room temperature. Dissolved ethyl (2-chloroacetyl)carbamate (1216 mg, 7.34 mmol) in acetonitrile and added to the reaction solution, then CS_2 (0.44 mL, 7.34 mmol) was added and stirred for 30 minutes. The reaction mixture was poured into water and extracted with DCM three times. The crude product was further purified by silica gel column chromatography (petroleum ether: DCM = 1:2) to afford compound 3 as light yellow solid. (1157 mg, 85.5%). ^{1}H NMR (400 MHz, $CDCl_3$) δ 7.49 (s, 1H), 7.36–7.32 (m, 3H), 7.28 (s,1H), 5.15 (s, 4H), 3.99 (s, 4H).

Compound 4. Compound 4 was synthesized follow the routes of literature[1].

Compound 5. Compound 4 (400 mg, 0.26 mmol) and 3-(2-ethylhexyl)-2-thioxothiazolidin-4-one (77 mg, 0.31 mmol) were added to a three-necked flask and dissolved in chloroform, then piperidine (0.51 mL, 5.21 mmol) was added dropwise to the reactant. The reaction mixture was heated to 50 °C and stirred for 6 hours. After cooling to room temperature, the reaction mixture was poured into water and extracted with DCM three times. The crude product was further purified by silica gel column chromatography (petroleum ether: DCM = 1:1) to afford compound 5 as a purplish-red solid. (260 mg, 56.6%).^{1}H NMR (400 MHz, $CDCl_3$) δ = 9.92 (s, 1H), 7.86 (s, 1H), 7.74 (s, 1H), 7.54 (s, 1H), 7.39 (d, *J*=3.6, 2H), 7.24 (d, *J*=2.8, 2H), 7.17 (s, 2H), 7.06 (s, 2H), 4.06 (d, *J*=7.2, 2H), 2.98–2.63 (m, 12H), 1.89–1.65 (m, 9H), 1.55–1.23 (m, 50H), 1.12–0.84 (m, 30H).

BDT-Dimer1. Compound 5 (150 mg, 0.09 mmol) and compound 2 (8.6 mg, 0.03 mmol) were added to a three-necked flask and dissolved in chloroform, then piperidine (0.25 mL, 2.55 mmol) was added dropwise to the reactant. The reaction mixture was heated to 65 °C and stirred overnight. After cooling to room temperature, the reaction mixture was poured into water and extracted with chloroform for three times. The crude product was further purified by silica gel column chromatography (petroleum ether: chloroform = 1:4) to afford BDT-Dimer2 as a purple solid (68.9 mg, 47.2%). ^{1}H NMR (400 MHz, $CDCl_3$) δ = 8.27 (s, 2H), 7.82 (s, 2H), 7.78 (s, 2H), 7.54 (s, 2H), 7.34 (s, 6H), 7.20 (s, 4H), 7.09 (s, 2H), 7.02 (s, 4H), 4.36 (t, *J*=6.2, 4H), 4.05 (d, *J*=7.2, 4H), 2.97–2.60 (m, 24H), 1.96–1.64 (m, 30H), 1.58–1.36 (m, 90H), 1.28 (s, 24H), 1.06–1.01 (m, 14H), 0.97–0.80 (m, 28H).

BDT-Dimer2. Compound 5 (150 mg, 0.09 mmol) and compound 1 (11.9 mg, 0.03 mmol) were added to a three-necked flask and dissolved in chloroform, then piperidine (0.25 mL, 2.55 mmol) was added dropwise to the reactant. The reaction mixture was heated to 65 °C and stirred overnight. After cooling to room temperature, the reaction mixture was poured into water and extracted with chloroform for three times. The crude product was further purified by silica gel column chromatography (petroleum ether: chloroform = 1:3) to afford BDT-Dimer1 as a purple solid (64.0 mg, 43.9%). ^{1}H NMR (400 MHz, $CDCl_3$) δ = 7.82 (s, 4H), 7.41–7.30 (m, 12H), 7.18 (s, 4H), 7.11 (s, 2H), 7.01 (s, 2H), 4.12 (t, *J*=7.5, 4H), 4.03 (d, *J*=7.3, 4H), 2.85–2.75 (m, 24H), 1.82–1.64 (m, 26H), 1.49–1.31 (m, 84H), 1.30–1.21 (m, 20H), 1.03–0.98 (m, 12H), 0.95–0.84 (m, 44H).

BDT-Dimer3. Compound 5 (200 mg, 0.11 mmol) and compound 3 (16.7 mg, 0.05 mmol) were added to a three-necked flask and dissolved in chloroform, then piperidine (0.34 mL, 3.40 mmol) was added dropwise to the reactant. The reaction mixture was heated to 65 °C and stirred overnight. After cooling to room temperature, the reaction mixture was poured into water and extracted with chloroform for three times. The crude product was further purified by silica gel column chromatography (petroleum ether: chloroform = 1:3) to afford BDT-Dimer3 as a purple solid (125.2 mg, 64.4%). ^{1}H NMR (400 MHz, $CDCl_3$) δ = 7.82 (s, 2H), 7.78 (s, 2H), 7.40–7.31 (m, 12H), 7.14 (s, 4H), 7.06–6.94 (m, 8H), 5.29

(s, 4H), 4.02 (d, *J*=7.3, 4H), 2.98–2.62 (m, 24H), 1.80–1.61 (m, 20H), 1.51–1.30 (m, 88H), 1.31–1.20 (m, 8H), 1.05–0.95 (m, 30H), 0.92–0.83 (m, 32H).

Characterization methods

Structure characterization

^{1}H NMR (400 MHz) spectra were obtained from a Bruker DMX-400 NMR Spectrometer, and TMS was used as an internal standard. All samples were dissolved in $CDCl_3$ and tested at room temperature. MALDI-TOF-MS spectra were obtained from a Micromass GCT-MS spectrometer.

DFT calculation

The optimized molecular structure and the electron density of the frontier energy levels were calculated by the density functional theory (DFT) method at the B3LYP/6-31G(d,p) level with Gaussian 09 program, and alkyl groups were replaced by methyl to simplify the calculations.

UV−vis absorption spectra and the measurement of T_g

The absorption spectra were tested on Perkin Elmer Lambda950 spectrophotometer. For film testing, the samples to be tested were prepared by spin coating on the quartz sheets. The samples were dissolved in CF with a concentration of ca. 12 mg mL^{-1}, and then spin-coated at a speed of 1500 rpm for 30 seconds. The measured thickness of films is approximately 65 nm. The glass transition temperature (T_g) was characterized by a change in the slope of the deviation metric (the sum of the squared deviation in absorbance between as-cast and annealed films) versus temperature, corresponding to the onset of the formation of photophysical aggregates due to molecular-scale rearrangement. And it was obtained by measuring the absorption spectra of the films during continuous annealing. All the test films were annealed at the corresponding temperature for ten minutes, and their absorption spectra were tested and collected at intervals of ten degrees Celsius. Then linear fitting was performed on the deviation metrics before and after glass transition, and the intersection of the two lines was the T_g value.

CV test

The cyclic voltammetry (CV) measurement was carried out by an electrochemical workstation (VMP3 Biologic, France) with Pt electrode coated with target films, Pt plate and Ag/Ag$^+$ electrode acting as the working, counter, and reference electrodes, respectively, in a 0.1 mol L^{-1} tetrabutylammonium phosphorus hexafluoride (Bu_4NPF_6) acetonitrile solution. Redox potentials were calibrated using the ferrocene/ferrocenium (Fc/Fc^+) redox couple (−4.8 eV).

Fluorescence spectra

The fluorescence spectra were tested on FluoroMax. For the solution, samples were dissolved in CF with a concentration of 1 μg mL^{-1} and the excited wavelength was 500 nm. The films were prepared through spin-coating with the thickness of *ca.* 65 and 100 nm for pure and blend films, respectively. And 530 nm and 650 nm were selected to excite the donor and acceptor in the film, respectively.

Contact angle measurement

Contact angles were measured with a contact angle meter (GBX DIGIDROP). The solution of each organic material was spin-coated on cleaned ITO substrates. Droplets of water, diiodomethane, and glycerol were dripped onto the different films. According to Owens-Wendt method, surface energy could be divided into dispersive and polar components.

$$\gamma = \gamma^d + \gamma^p$$

Furthermore, the dispersive and polar surface energy can be calculated through the formula below based on the contact angles obtained by two solvents.

$$(1 + \cos\theta)\,\gamma_L = 2\sqrt{\gamma_S^d \gamma_L^d} + 2\sqrt{\gamma_S^p \gamma_L^p}$$

where θ is the contact angle of a specific solvent, is the surface energy of the solvent, and refers to the dispersive and polar surface energy of the solid, respectively, and and refers to the dispersive and polar surface energy of the solvent, respectively. Thus, the unknown value and can be solved though combining two equations obtained by contact angle measurement of two different solvents. Solubility parameter (δ) can be calculated from the surface energy,

$$\delta = K\sqrt{\gamma}$$

where γ is the surface energy, K is the proportionality constant ($K = 116 \times 10^3$ $m^{-1/2}$). And Flory–Huggins interaction parameter (χ_{ij}) can be written as a function of two solubility parameter,

$$\chi_{ij} = \frac{V_0}{RT}(\delta_i - \delta_j)^2$$

where χ_{ij} is the Flory–Huggins interaction parameter between the material i and j, V_0 is the geometric mean of the polymer segment molar volume, R is the gas constant, T is the absolute temperature, and

and are the solubility parameter of material i and j, respectively. To simplify, we define the parameter $\kappa = K^2 V_0/RT$, then the Flory–Huggins interaction parameter can be written as the formula below,

$\chi_{ij} = \kappa\,(\sqrt{\gamma_i} - \sqrt{\gamma_j})^2$

where and are the surface energy of material i and j, respectively.

Spin-coating in-situ UV–visible-NIR spectroscopy

A specially designed spin coater, which allows the detective beam to pass through the center of the fabricating devices, was applied to measure the *in-situ* UV–vis spectrum. An F-20 spectrometer from filmetrics was used to record the spectrum, and the time resolution of the spectrum is 5 ms. All data presented and analyzed was processed using savgol-filter from a scipy kit to remove the periodic change in the spectrum brought by the spinning of ITO stripe during fabrication[2].

Device fabrication and characterization

The photovoltaic devices were fabricated with a conventional structure of ITO/PEDOT:PSS/Active layer /PNDIT-F3N/Ag. The ITO-coated glass substrates with a sheet resistance of ≈15 Ω were sonicated in detergent, deionized water, alcohol, and isopropanol for 30 min each sequentially. After drying, the substrates were treated with UV-ozone for 15 min. The PEDOT:PSS layer was prepared through spin coating at 3500 rpm for 30s. Then, the PEDOT:PSS substrates were subsequently baked in air at 150 °C for 15 min. An additive, 1-bromo-3,5-dichlorobenzene (DCBB) was dissolved in chloroform to prepare a solution with a concentration of 12 mg/mL. The donor and acceptor (D/A 1.5:1) were dissolved in above chloroform solution of DCBB with a total concentration of 15 mg mL^{-1}. And then, the blend solution was stirred at 50 °C for 1.5 hours. The active layer was spin-coated at a speed of 1400 rpm for 30 seconds from the blend solution. After TA treatment, PNDIT-F3N methanol solution (0.5 mg mL^{-1}) was spin-coated at 3000 rpm for 30 s on the active layer. Finally, a layer of ca. 160 nm Ag layer was evaporated onto the active layer under high vacuum ($<1 \times 10^{-4}$ Pa).

Device *J-V* characterization was conducted under AM 1.5 G (100 mW cm^{-2}) using a Newport Thermal Oriel 91159A solar simulator in a glovebox of nitrogen atmosphere. Light intensity is calibrated with a Newport Oriel PN 91150V Si-based solar cell. *J–V* characteristics were recorded using a Keithley 2400 source-measure unit. Typical cells have device areas of 4 mm^2, and we also confirmed the device performance with a mask of 2.56 mm^2.

EQE spectrum was measured through the Solar Cell Spectral Response Measurement System FETOS-QE-3011 (Enli Technology Co., Ltd., Taiwan).

Transient photocurrent (TPC) were measured by applying a 488 nm solid state laser (Coherent OBIS CORE 488LS) with a pulse width of ca. 30 ns. The current traces were recorded using a mixed domain oscilloscope (Tektronix MDO3032) by measuring the voltage drop across a 2 Ω resistor load connected in series with the solar cell.

Photocurrent density (J_{ph}) and effective voltage (V_{eff}) test was used to characterize the utilization efficiency of photons. V_{eff} equals the the applied bias minus the voltage where photocurrent is zero, and J_{ph} represents the current density differences between illumination and dark. At a sufficiently high V_{eff}, it is assumed that all excitons are dissociated into free charges, and the photogenerated current reaches the maximum saturation (J_{sat}). The exciton dissociation efficiency (P_{diss}) and charge collection efficiency (P_{coll}) of the device can be calculated from the J_{ph}/J_{sat} values under short-circuit and maximum power output conditions, respectively.

Power index α in supplementary Fig. 14 fitted from the function of $J \propto (P_{light})^{\alpha}$, in which P_{light} represents the light intensity; ideal factor n in Fig. 5e fitted from the function of $V_{OC} \propto nkT\log(P_{light})$, where k is the Boltzmann constant, T is the temperature in Kelvin.

Charge carrier mobility characterization

The mobility of hole and electron was tested by fitting the current-bias characteristics in the dark utilizing a field-independent space charge limited current (SCLC) model following the Mott-Gurney law:

$$J = \frac{9\varepsilon_0\varepsilon_r\mu V^2}{8L^3} exp(0.89\beta\sqrt{\frac{V - V_{bi}}{L}})$$

The structures of hole-only and electron-only devices are ITO/PEDOT:PSS/Active layer/MoO_3/Ag and ITO/ZnO/Active layer/PNDIT-F3N/Ag, respectively. The active layers for these two devices were spin-coated under the same conditions as those of solar cells. J–V curves in the range of 0 to 5 V were gained by Keithley 2400 source-measure unit in the dark condition.

Energy loss measurement

Fourier-transform Photocurrent spectroscopy external quantum efficiency (FTPS-EQE) and Electroluminescence quantum efficiency (EQE_{EL}) measurements. FTPS-EQE was conducted by an integrated system with Fourier transform Photocurrent meter (PECT-600, Enlitech). EQE_{EL} measurement was performed by applying external voltage/current sources through the devices (REPS, Enlitech).

Morphology and crystallization characterization

Transmission electron microscopy (TEM) characterization was performed by Tecnai G2 F20 U-TWIN TEM instrument. AFM measurements were performed on Multimode 8 with ScanAsyst mode. Grazing incidence wide angle X-ray scattering (GIWAXS) measurement was conducted at XEUSS WAXS equipment.

Supplementary Figures

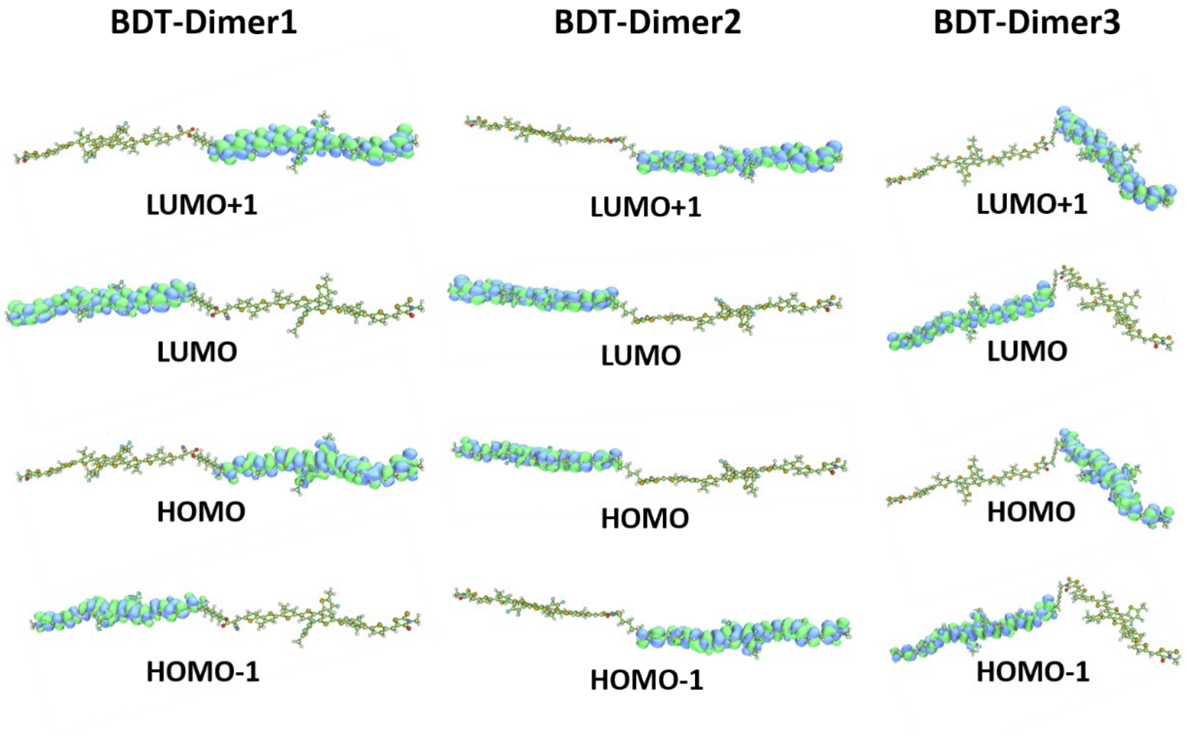

Figure S1. DFT-calculated electron density distribution in the frontier energy levels of BDT-Dimers.

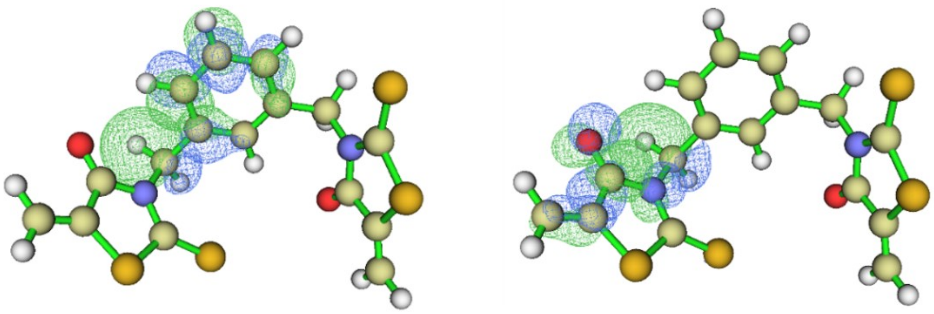

Figure S2. DFT-calculated NBO analyses for hyperconjugation effect in linker of BDT-Dimer3.

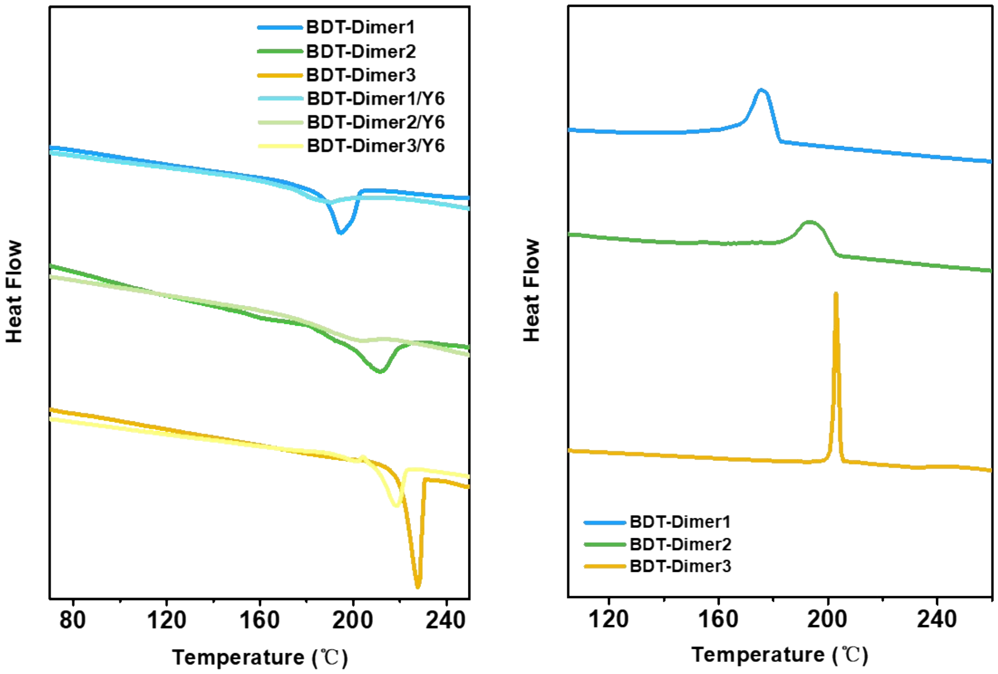

Figure S3. DSC curves of BDT-Dimers and blends.

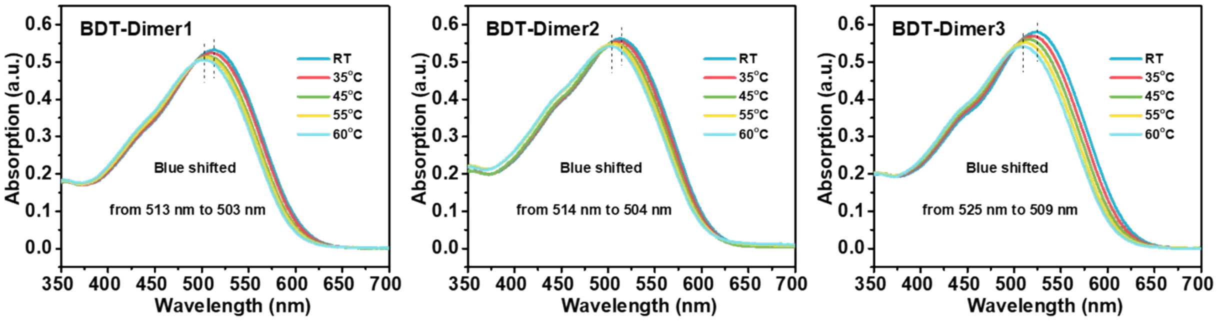

Figure S4. Temperature-dependent solution absorption of BDT-Dimers.

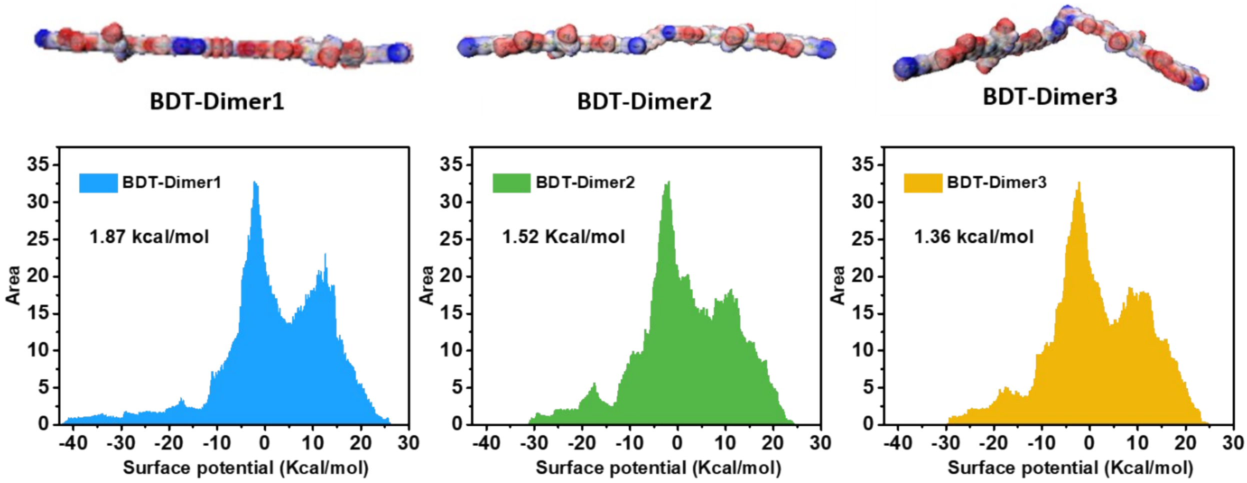

Figure S5. DFT-calculated ESP distribution and average ESP of BDT-Dimers.

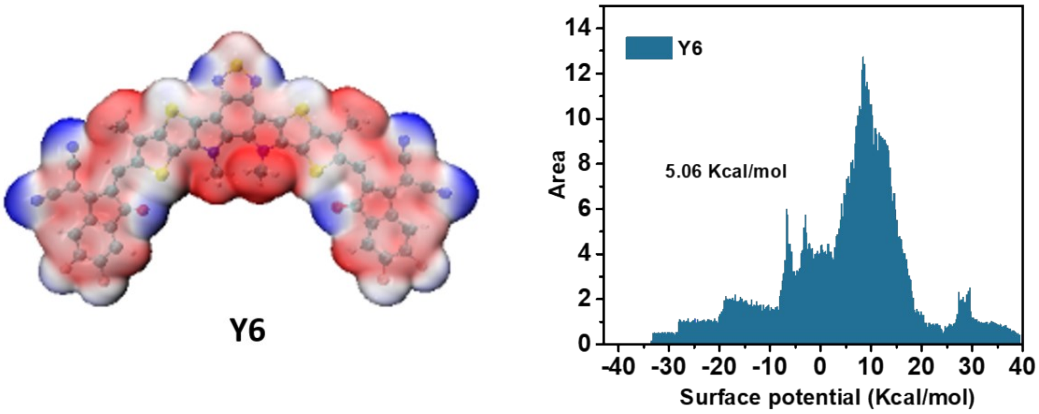

Figure S6. DFT-calculated ESP distribution and average ESP of Y6.

Figure S7. Contact angles of BDT-Dimers and Y6.

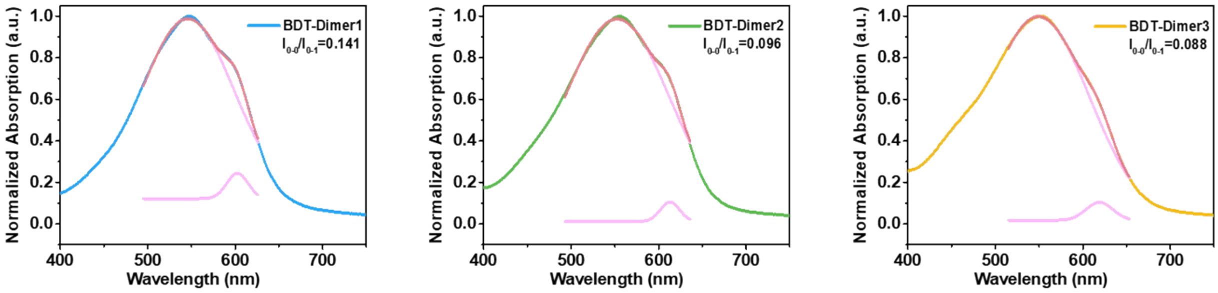

Figure S8. Peak fitting for film absorption spectra of BDT-Dimers.

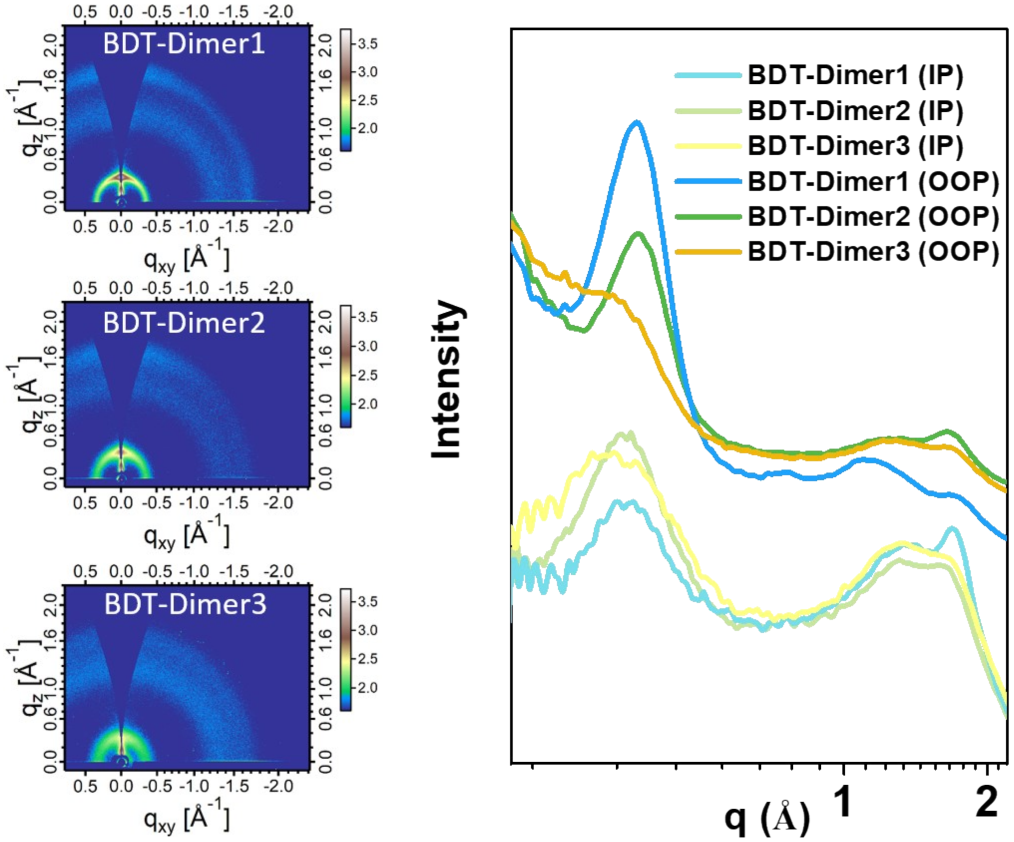

Figure S9. 2-D and corresponding 1-D GIWAXS of BDT-Dimers without TA.

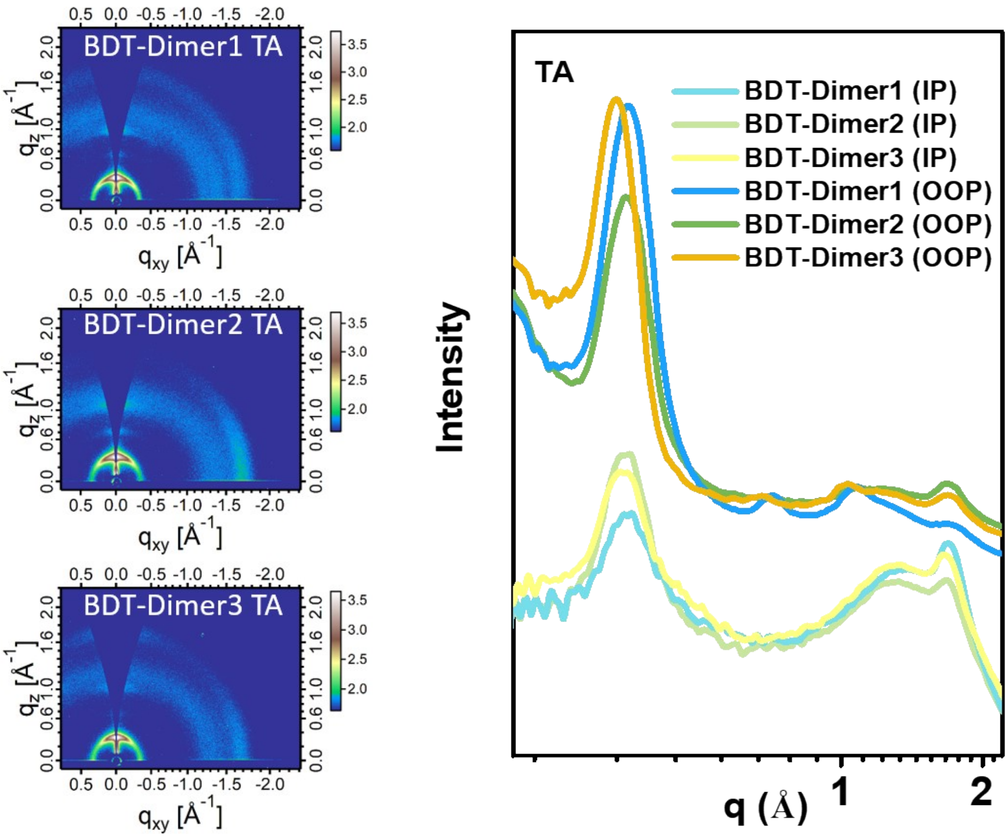

Figure S10. 2-D and corresponding 1-D GIWAXS of BDT-Dimers after TA.

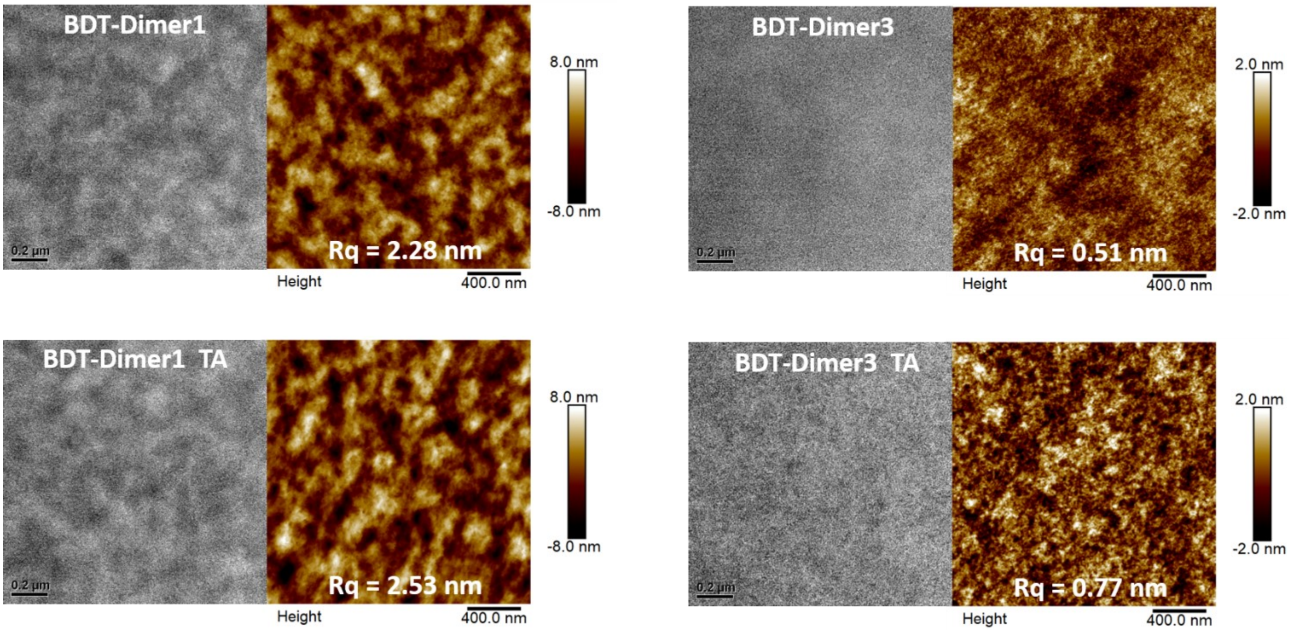

Figure S11. TEM and AFM images for pure BDT-Dimer1 and BDT-Dimer3 films before and after TA treatment.

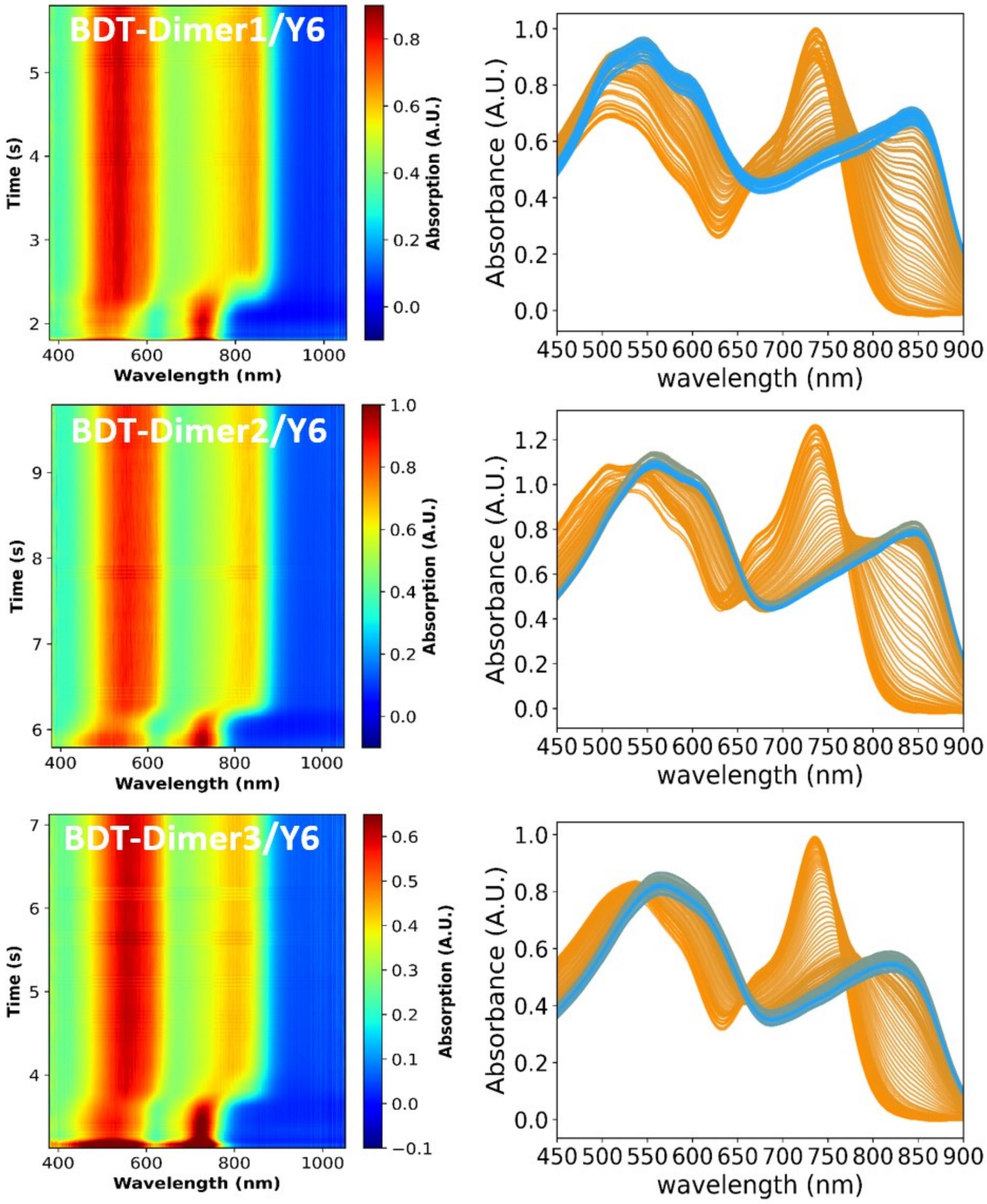

Figure S12. 2-D and corresponding 1-D in-situ UV–visible-NIR spectroscopy of BDT-Dimers/Y6 during spin-coating.

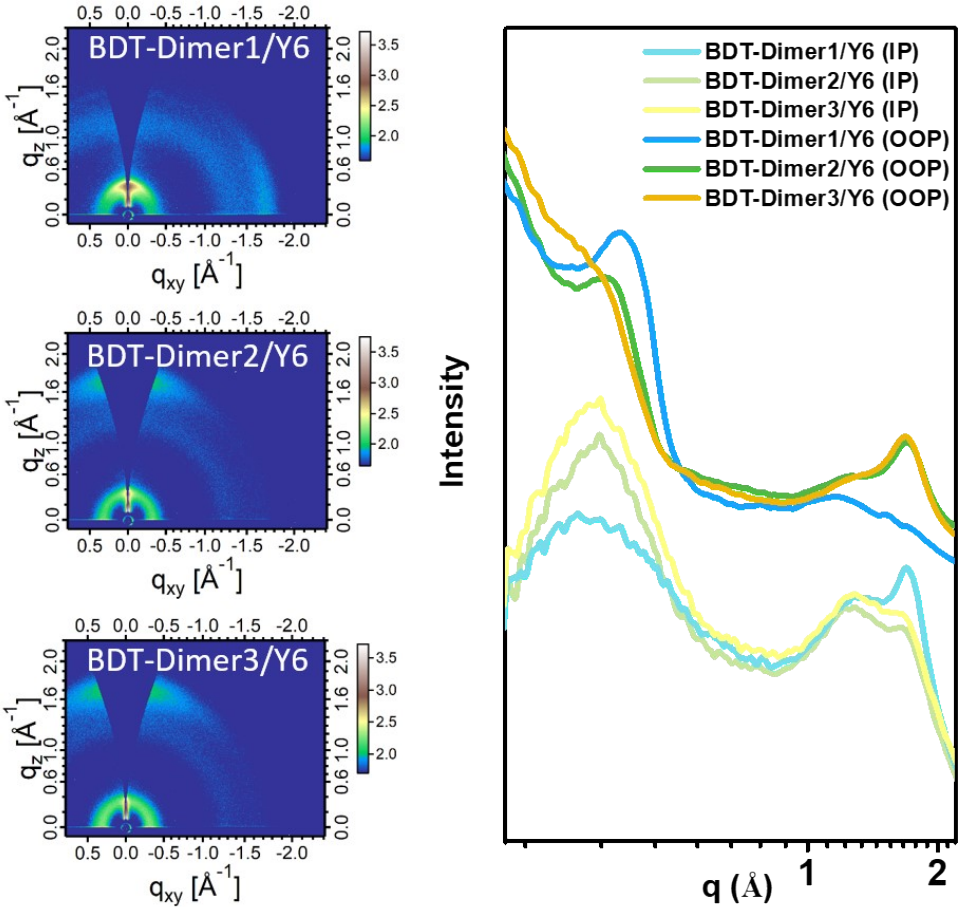

Figure S13. 2-D and corresponding 1-D GIWAXS of BDT-Dimers/Y6 blends without TA.

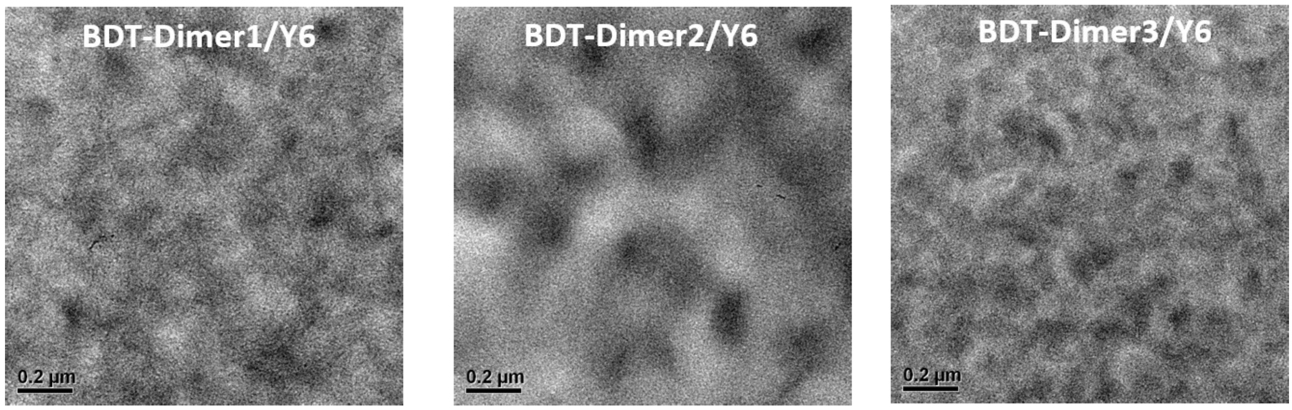

Figure S14. TEM images based on BDT-Dimers/Y6 blends without TA.

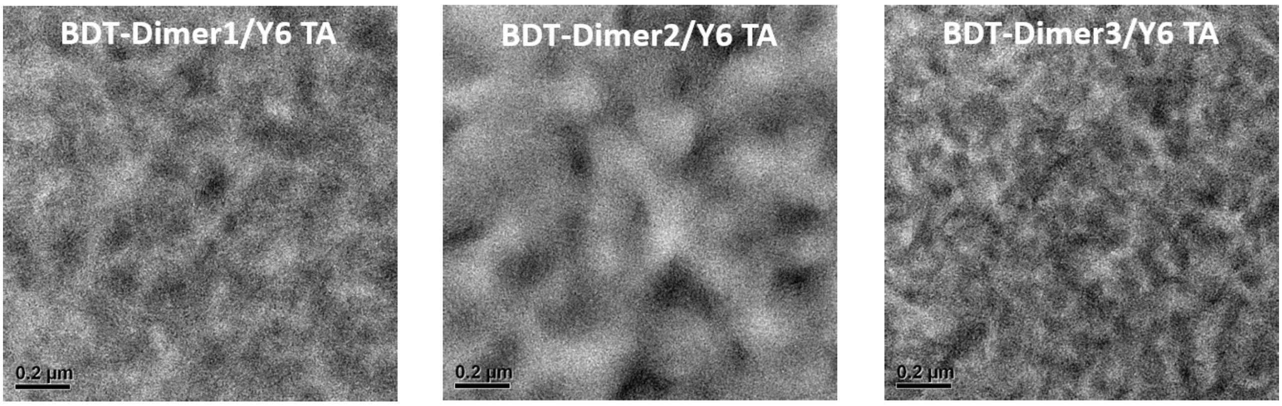

Figure S15. TEM images based on optimized BDT-Dimers/Y6 blends.

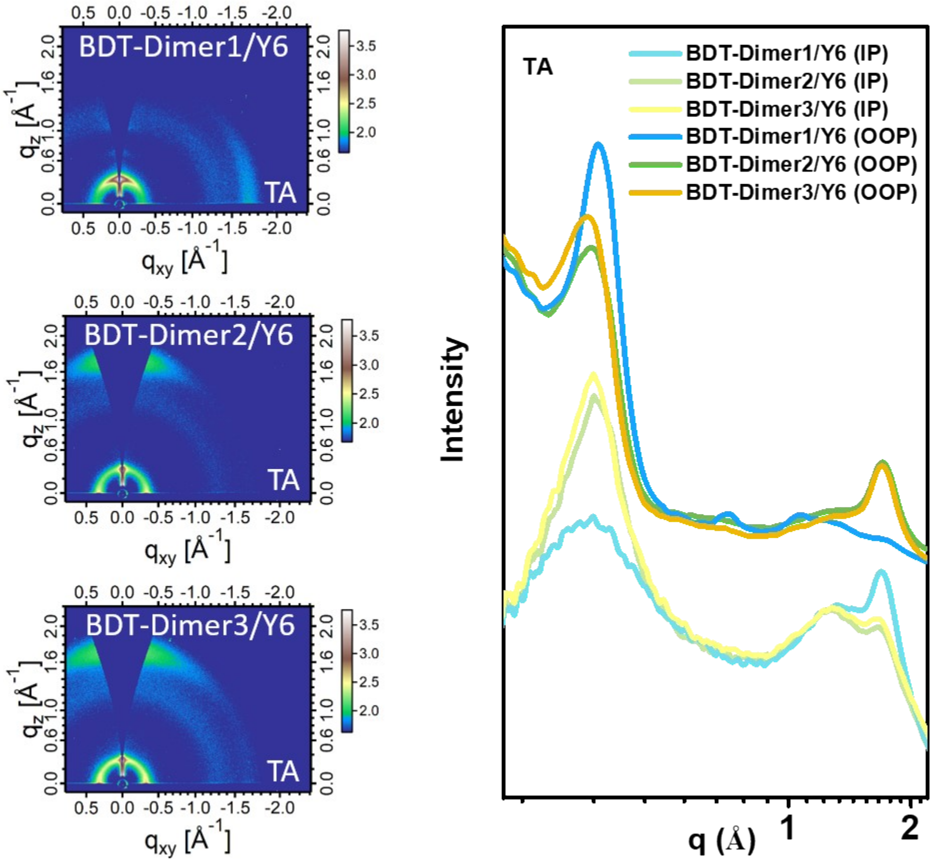

Figure S16. 2-D and corresponding 1-D GIWAXS of optimized BDT-Dimers/Y6 blends.

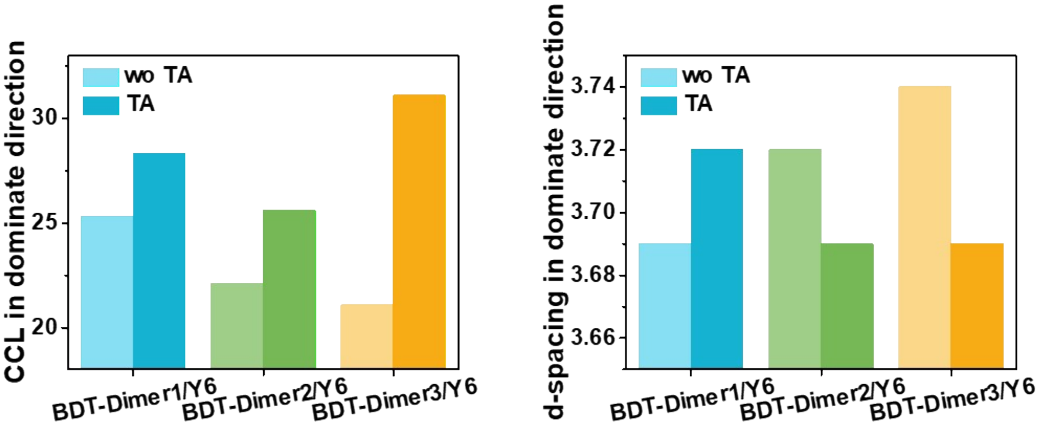

Figure S17. CCL and d-spacing with/without TA in dominate direction of BDT-Dimers/Y6 blends.

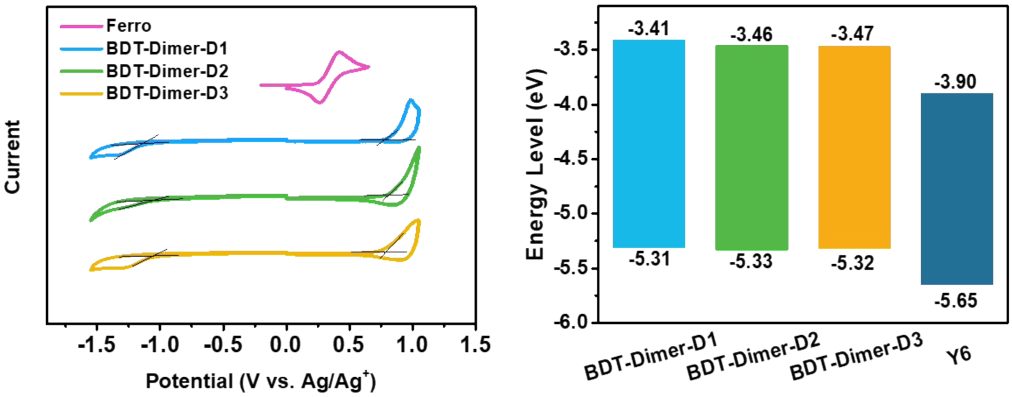

Figure S18. CV curves of the BDT-Dimers and calculated frontline orbital energy level.

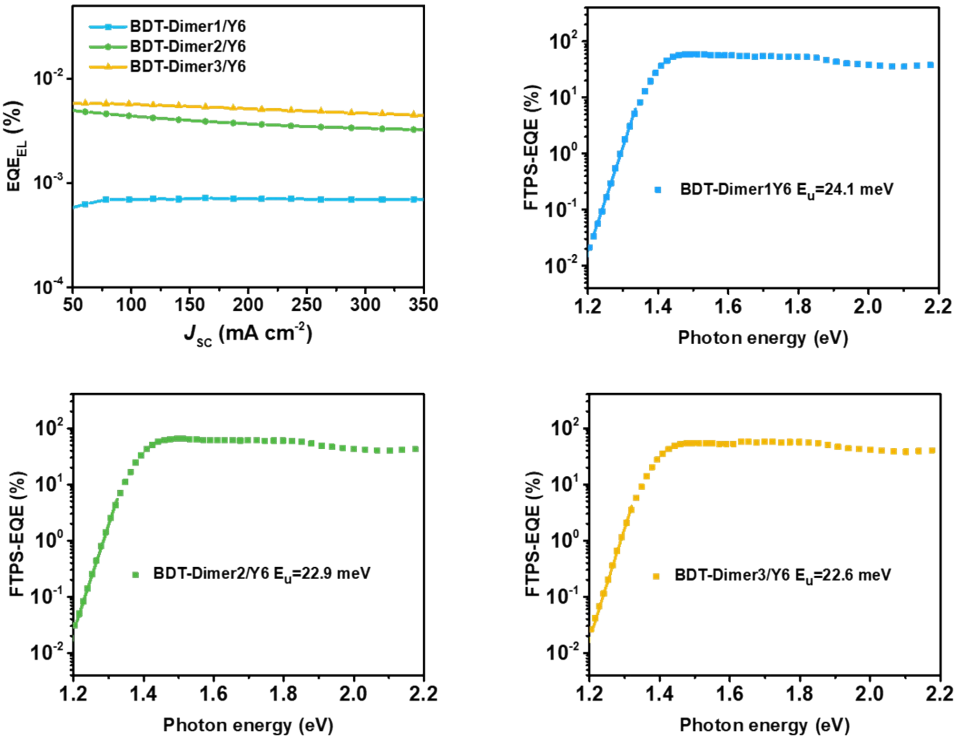

Figure S19. EQE_{EL} and E_u of optimized devices based on BDT-Dimers/Y6.

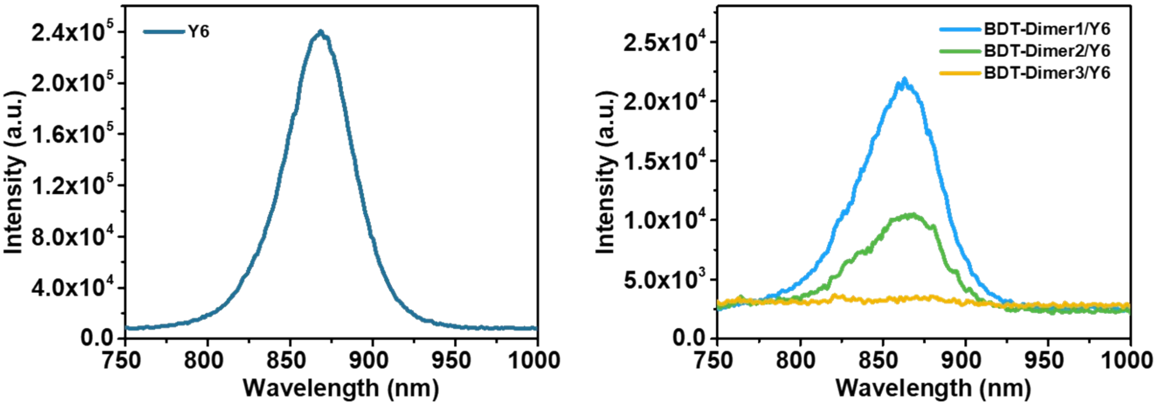

Figure S20. Fluorescence emission spectra of Y6 and BDT Dimers/Y6 films.

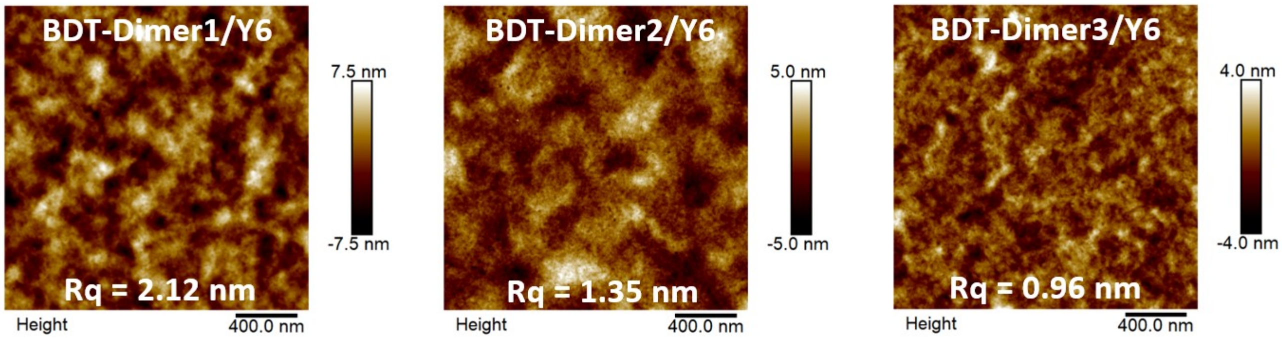

Figure S21. AFM height images based on optimized BDT-Dimers/Y6 blends.

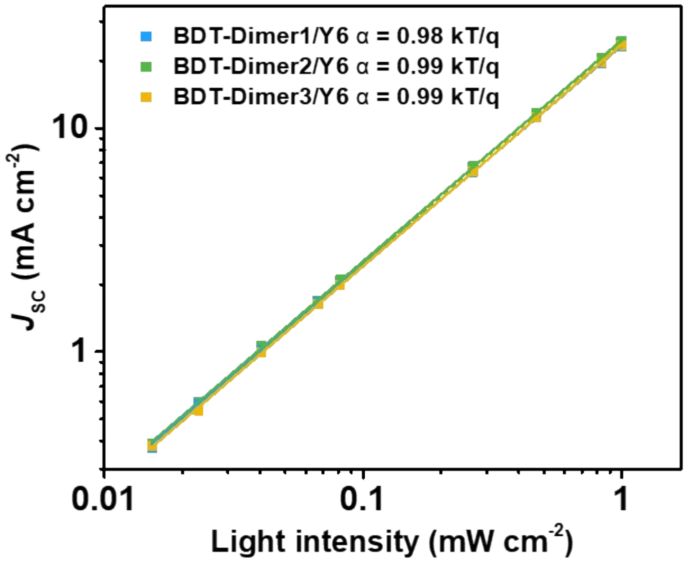

Figure S22. Fitting straight lines of J_{SC} with changes in light intensity.

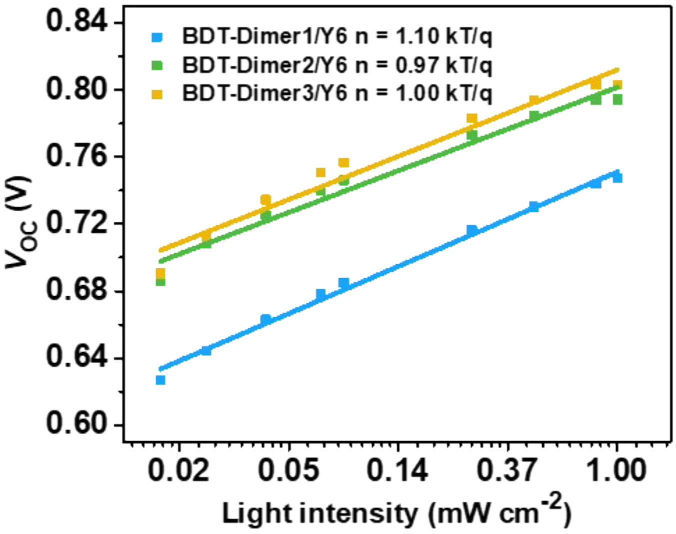

Figure S23. Fitting straight lines of V_{OC} with changes in light intensity.

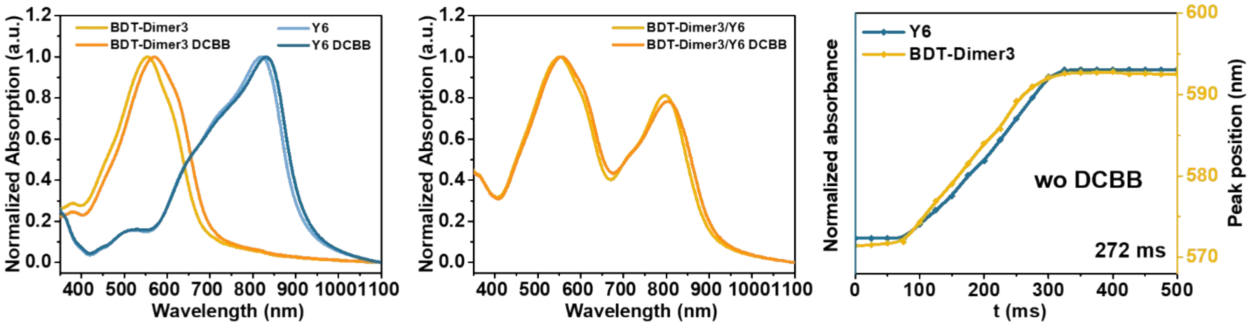

Figure S24. Absorption of BDT-Dimer3, Y6 and BDT-Dimer3/Y6 films with/without DCBB addition, and UV-visible-NIR of BDT-Dimer3/Y6 blends without DCBB addition.

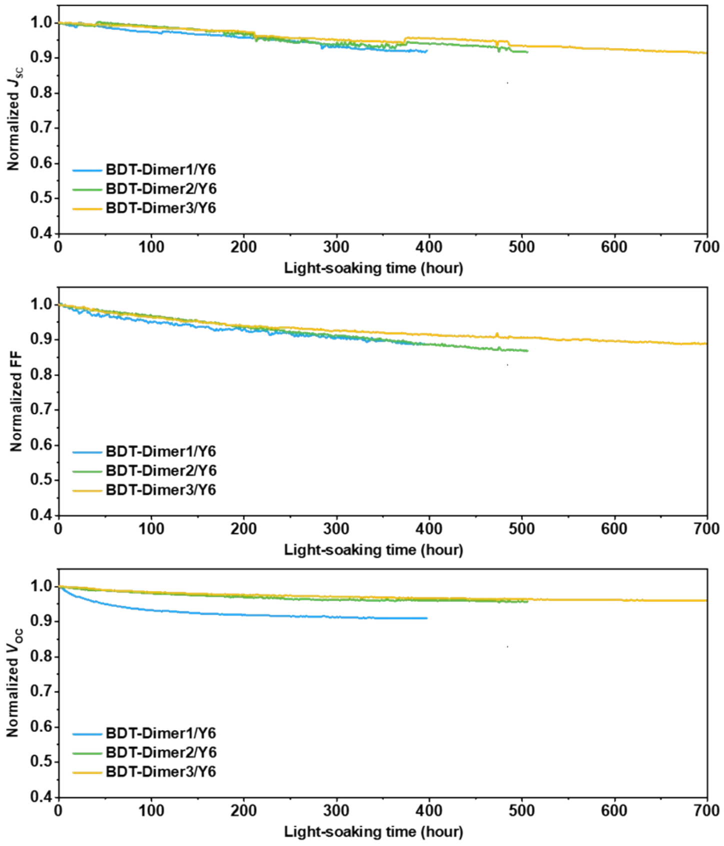

Figure S25. Normalized J_{SC}, FF and V_{OC} with light irradiation for optimized devices.

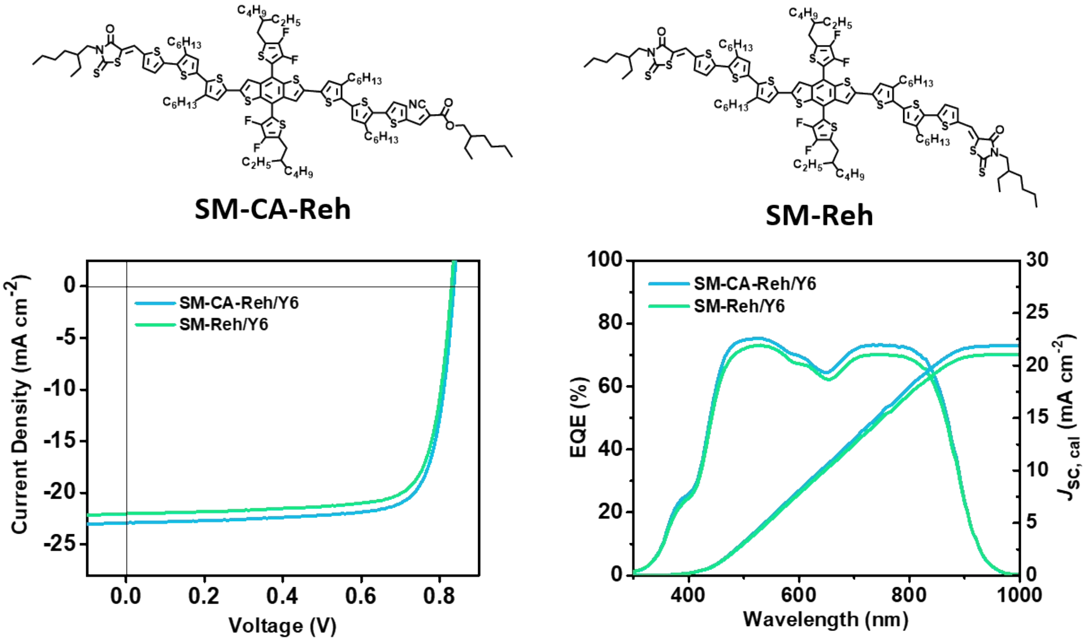

Figure S26. Chemical structures of SM-CA-Reh and SM-Reh, and their optimized *J*-*V* and EQE curves pairing with Y6.

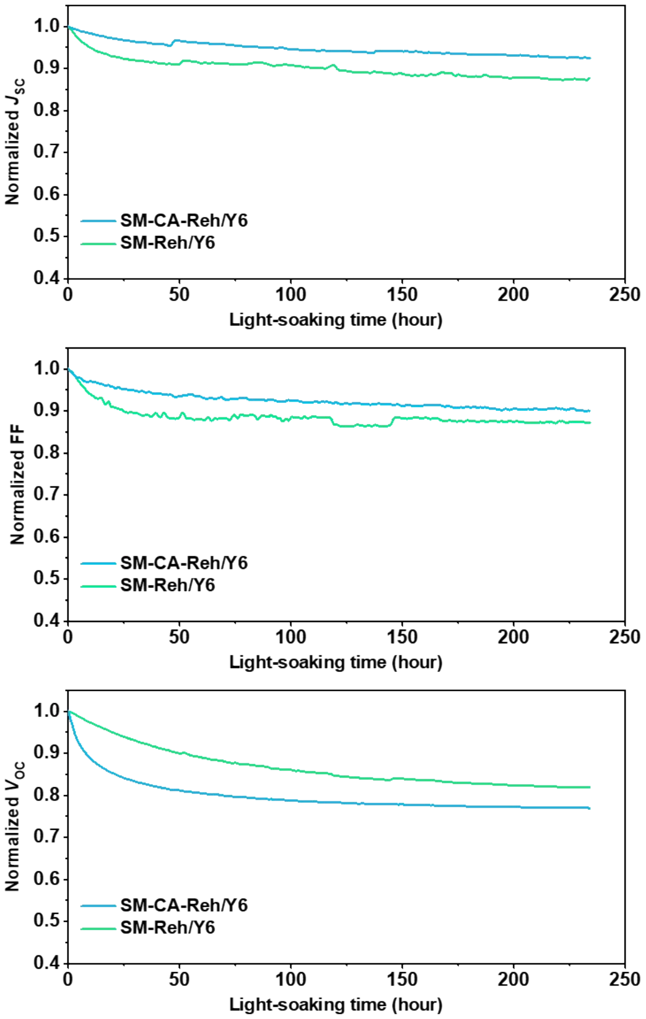

Figure S27. Normalized J_{SC}, FF and V_{OC} with light irradiation for optimized devices based on SM-CA-Reh/Y6 and SM-Reh/Y6.

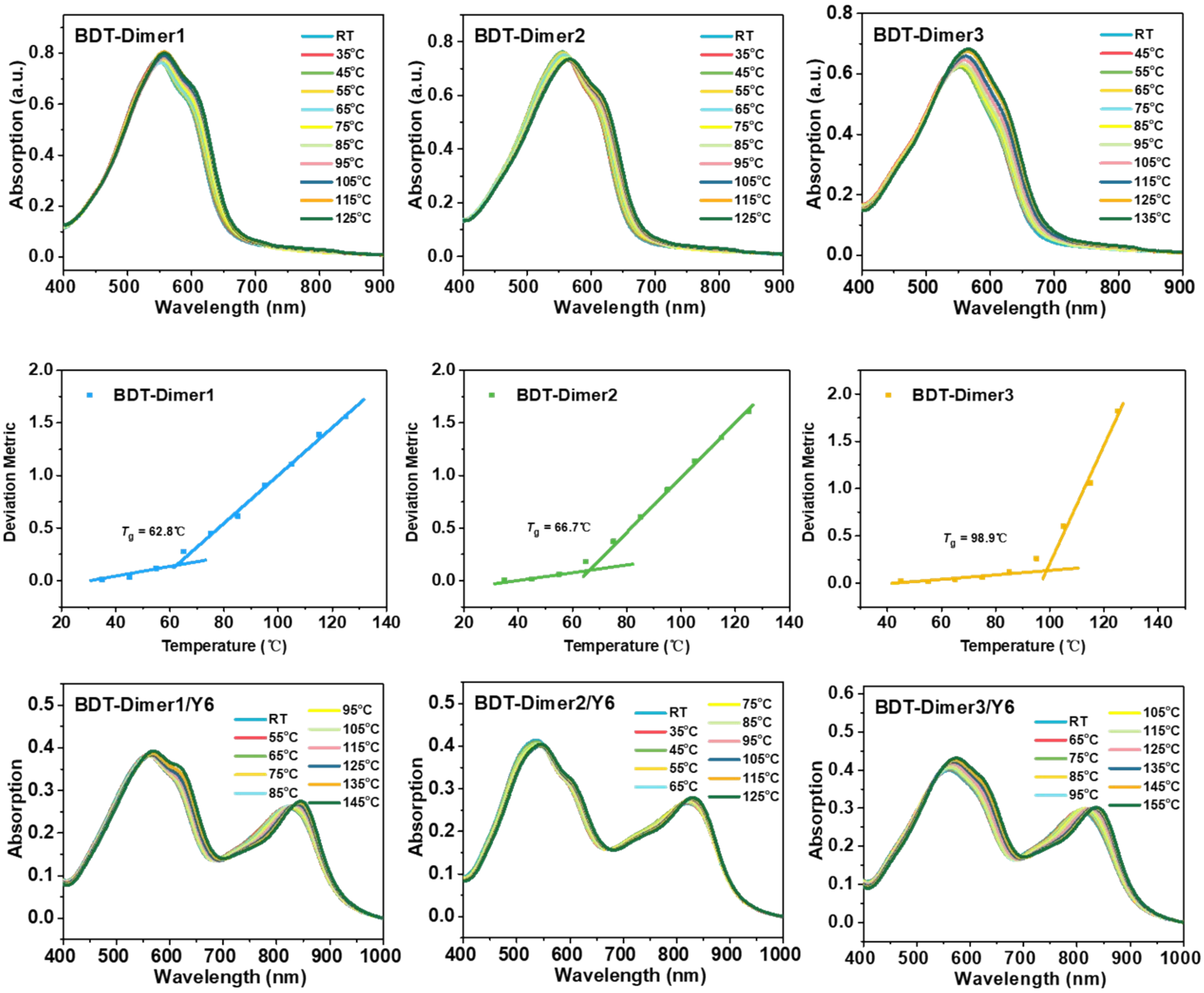

Figure S28. Film absorption of BDT-Dimers and BDT-Dimers/Y6 blends during continuous annealing and T_g of BDT-Dimers.

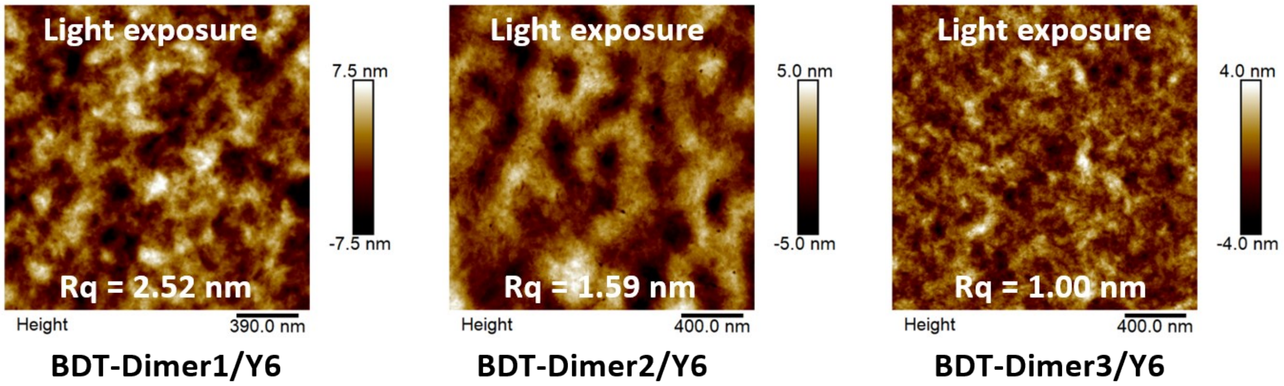

Figure S29. AFM height images based on optimized BDT-Dimers/Y6 blends under light soaking for 48 hours.

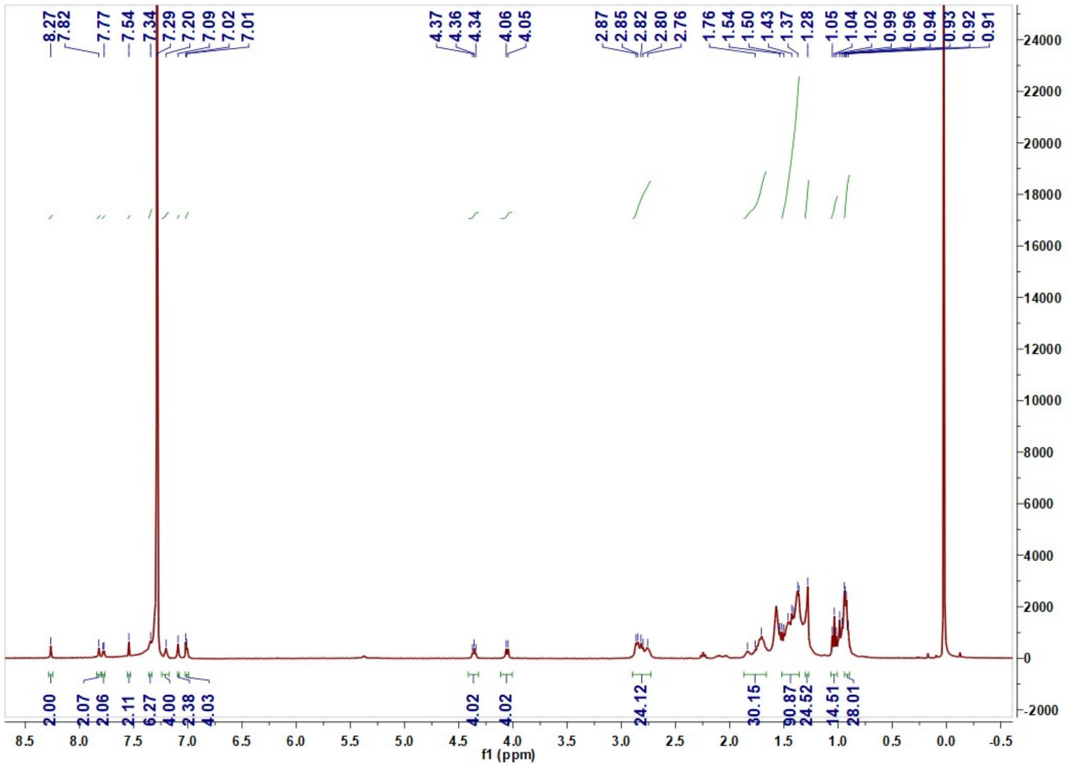

Figure S30. ^{1}H NMR spectrum of BDT-Dimer1 in $CDCl_3$.

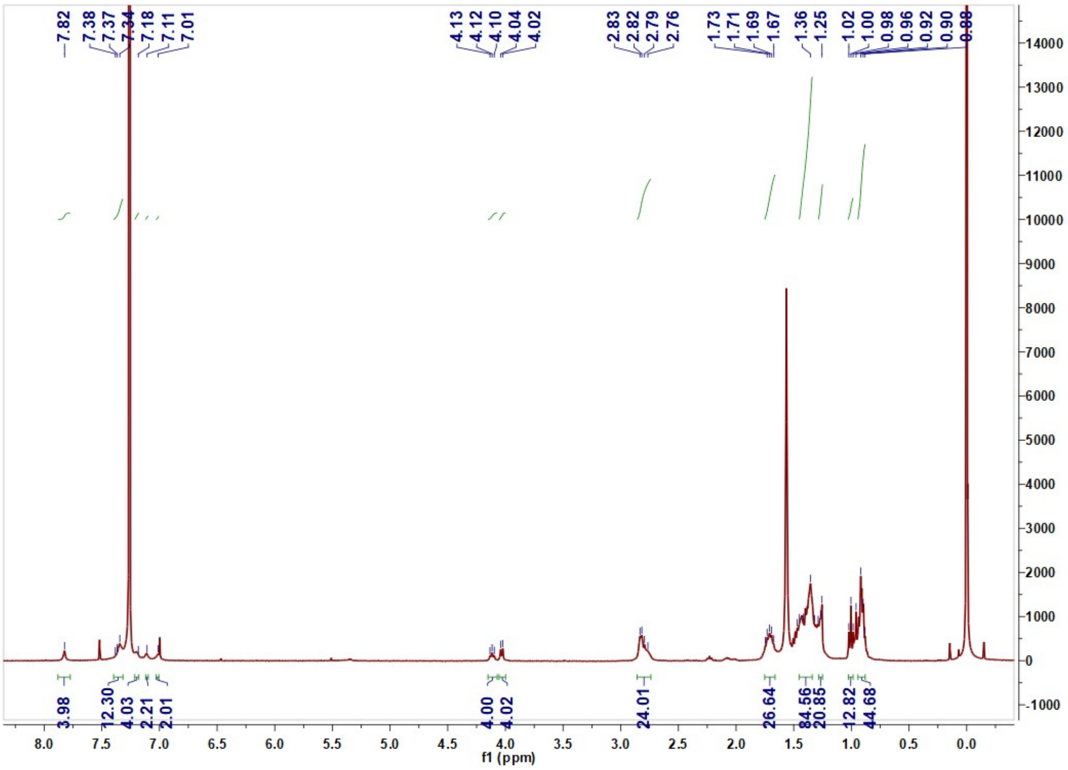

Figure S31. ^{1}H NMR spectrum of BDT-Dimer2 in $CDCl_3$.

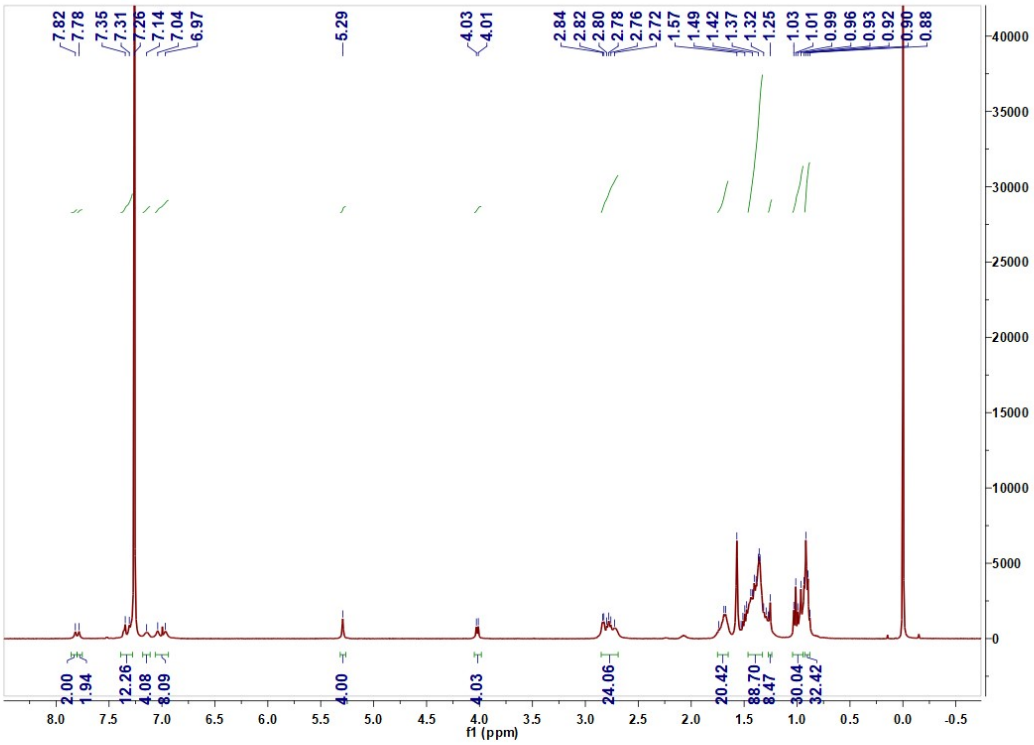

Figure S32. ^{1}H NMR spectrum of BDT-Dimer3 in $CDCl_3$.

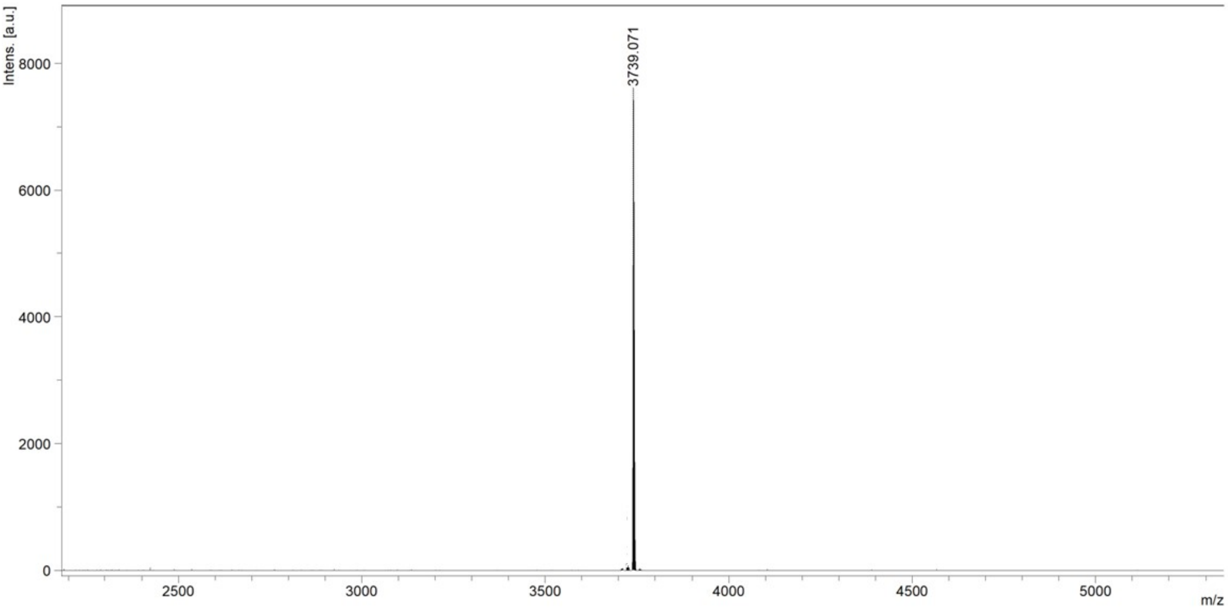

Figure S33. MALDI-TOF-MS spectrum of BDT-Dimer1.

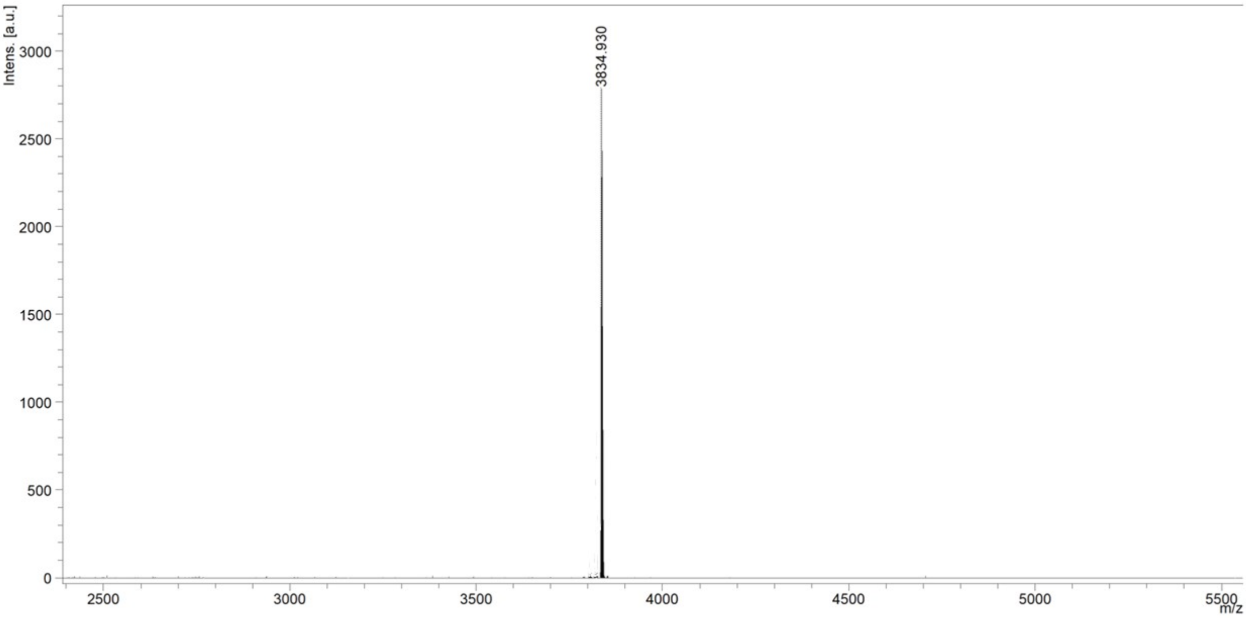

Figure S34. MALDI-TOF-MS spectrum of BDT-Dimer2.

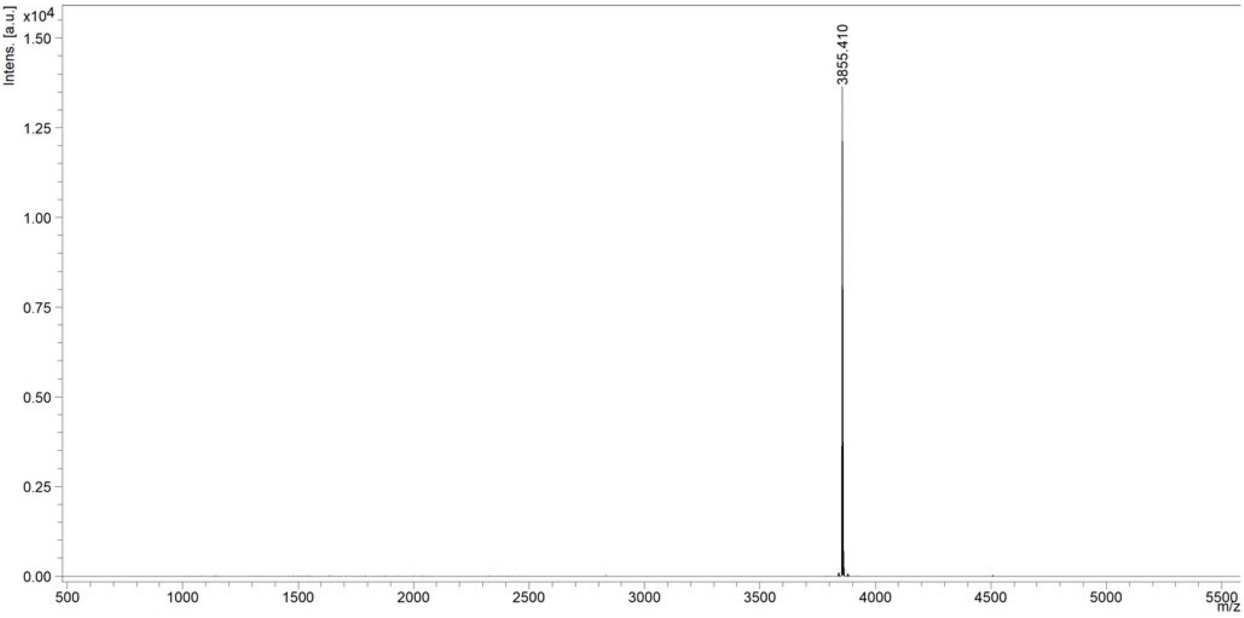

Figure S35. MALDI-TOF-MS spectrum of BDT-Dimer3.

Supplementary Tables

Supplementary Tables

Table S1. Detailed data extracted from DSC of pure donors and blends.

Materials	T_m (°C)	$T_{m,mix}$ (°C)	ΔH_m (J/g)	T_C (°C)	ΔG_{ls} (J/g)	χ
BDT-Dimer1	194.3	189.9	−15.7	175.8	−1.49	2.14
BDT-Dimer2	211.5	202.4	−16.4	193.5	−1.40	1.71
BDT-Dimer3	228.3	218.9	−22.8	203.2	−2.51	1.46

Table S2. Surface tension (Υ) and calculated Flory–Huggins interaction parameter (χ) calculated from contact angle.

Materials	BDT-Dimer1	BDT-Dimer2	BDT-Dimer3	Y6
Υ(mN m^{-1})	12.40	12.90	13.65	16.84
χ (Y6)	0.34	0.26	0.17	/

Table S3. Detailed data of GIWAXS for pristine donors with/without TA.

		OOP direction			**IP direction**		
		peak (Å^{-1})	***d*-spacing (Å)**	**CCL (Å)**	**peak (Å^{-1})**	***d*-spacing (Å)**	**CCL (Å)**
BDT-Dimer1	**wo TA**	0.364	17.2	99.3	0.352	17.8	61.0
		1.71	3.67	12.5	1.69	3.72	25.8
	TA	0.353	17.8	131.6	0.351	17.9	96.3
		1.66	3.78	12.4	1.69	3.72	27.7
BDT-Dimer2	**wo TA**	0.369	17.0	85.3	0.347	18.1	72.5
		1.64	3.82	19.1	1.64	3.83	18.6
	TA	0.349	17.9	118.3	0.347	18.1	113.3
		1.68	3.74	23.4	1.67	3.76	24.0
BDT-Dimer3	**wo TA**	0.314	20.0	44.8	0.327	19.2	49.6
		1.68	3.74	15.8	1.63	3.85	16.9
	TA	0.331	19.0	154.4	0.343	18.3	99.7
		1.69	3.72	24.6	1.68	3.74	26.6

Table S4. Detailed data of GIWAXS for blend films with/without TA

		OOP direction			IP direction		
		peak (Å^{-1})	***d*-spacing (Å)**	**CCL (Å)**	**peak (Å^{-1})**	***d*-spacing (Å)**	**CCL (Å)**
BDT-Dimer1/Y6	**wo TA**	0.368	17.1	47.8	0.312	20.1	42.5
		/	/	/	1.70	3.69	25.3
	TA	0.342	18.4	133.5	0.325	19.3	53.5
		1.70	3.69	15.4	1.69	3.72	28.3
BDT-Dimer2/Y6	**wo TA**	0.340	18.5	63.2	0.327	19.2	58.5
		1.69	3.72	22.1	1.64	3.82	17.2
	TA	0.323	19.4	74.3	0.338	18.6	91.7
		1.70	3.69	25.6	1.66	3.78	19.9
BDT-Dimer3/Y6	**wo TA**	/	/	/	0.321	19.6	54.7
		1.68	3.74	21.0	1.63	3.85	16.4
	TA	0.318	19.7	65.0	0.331	19.0	105.4
		1.70	3.69	31.1	1.65	3.81	21.6

Table S5. Device optimization of the ratios between donor and acceptor.

Active layer	**D:A**	V_{OC} **(V)**	J_{SC} **(mA/cm^2)**	**FF(%)**	**PCE (%)**
BDT-Dimer1/Y6	1.7:1	0.751	22.40	65.53	11.03
BDT-Dimer1/Y6	1.5:1	0.760	22.57	65.00	11.15
BDT-Dimer1/Y6	1.2:1	0.759	22.01	64.03	10.69
BDT-Dimer2/Y6	1.7:1	0.794	25.10	67.29	13.41
BDT-Dimer2/Y6	1.5:1	0.776	26.41	66.20	13.57
BDT-Dimer2/Y6	1.2:1	0.753	27.30	64.19	13.20
BDT-Dimer3/Y6	1.7:1	0.794	25.51	73.87	14.96
BDT-Dimer3/Y6	1.5:1	0.797	26.28	73.30	15.36
BDT-Dimer3/Y6	1.2:1	0.798	26.34	71.75	15.08

Table S6. Device optimization of TA temperature.

Active layer	**TA temperature**	V_{OC} **(V)**	J_{SC} **(mA/cm^2)**	**FF(%)**	**PCE (%)**
BDT-Dimer1/Y6	115°C	0.765	22.32	63.62	10.87
BDT-Dimer1/Y6	120°C	0.755	22.71	65.33	11.20
BDT-Dimer1/Y6	125°C	0.749	22.34	60.25	10.08
BDT-Dimer2/Y6	125°C	0.780	26.55	65.28	13.52
BDT-Dimer2/Y6	135°C	0.778	26.40	66.30	13.63
BDT-Dimer2/Y6	145°C	0.753	27.30	64.19	13.20
BDT-Dimer3/Y6	140°C	0.807	25.38	73.93	15.15
BDT-Dimer3/Y6	145°C	0.798	25.72	74.07	15.21
BDT-Dimer3/Y6	150°C	0.795	26.69	69.57	14.75

Table S7. Device optimization of DCBB concentration.

Active layer	DCBB	V_{OC} (V)	J_{SC} (mA/cm^2)	FF(%)	PCE (%)
BDT-Dimer1/Y6	14mg/ml	0.751	22.40	65.53	11.03
BDT-Dimer1/Y6	12mg/ml	0.758	23.13	65.21	11.44
BDT-Dimer1/Y6	10mg/ml	0.750	22.85	64.32	11.02
BDT-Dimer1/Y6	/	0.752	22.03	63.89	10.58
BDT-Dimer2/Y6	14mg/ml	0.764	26.88	66.33	13.63
BDT-Dimer2/Y6	12mg/ml	0.794	26.34	68.87	14.40
BDT-Dimer2/Y6	10mg/ml	0.780	26.55	65.28	13.52
BDT-Dimer2/Y6	/	0.791	25.67	65.10	13.22
BDT-Dimer3/Y6	14mg/ml	0.798	25.80	73.45	15.12
BDT-Dimer3/Y6	12mg/ml	0.800	27.39	71.56	15.68
BDT-Dimer3/Y6	10mg/ml	0.801	26.73	71.22	15.25
BDT-Dimer3/Y6	/	0.795	25.99	68.56	14.17

Table S8. Voltage loss of optimized devices.

Devices	**V^{cal}_{OC} (V)**	**E_g^{PV} (eV)**	**EQE_{EL} (%)**	**qV^{SQ}_{OC} (eV)**	**qV^{rad}_{OC} (eV)**	**E_{loss} (eV)**	**ΔE_1 (eV)**	**ΔE_2 (eV)**	**ΔE_3 (eV)**	**V_{OC} (V)**
BDT-Dimer1/Y6	0.756	1.416	5.78E-04	1.154	1.068	0.660	0.262	0.086	0.312	0.758
BDT-Dimer2/Y6	0.791	1.383	4.17E-03	1.123	1.052	0.592	0.260	0.071	0.261	0.789
BDT-Dimer3/Y6	0.796	1.384	4.74E-03	1.125	1.053	0.589	0.259	0.072	0.258	0.798

Table S9. Optimization of SM-CA-Reh/Y6 and SM-Reh/Y6 based devices.

Active layer	**Condition**	**V_{OC} (V)**	**J_{SC} (mA/cm^2)**	**FF(%)**	**PCE (%)**
SM-CA-Reh/Y6	SVA CS_2	0.832	20.69	75.66	13.02
SM-CA-Reh/Y6	SVA THF	0.827	20.71	68.34	11.71
SM-CA-Reh/Y6	SVA CF	0.802	19.51	71.06	11.12
SM-Reh/Y6	SVA CS_2	0.833	21.60	74.04	13.33
SM-Reh/Y6	SVA THF	0.791	19.42	71.01	10.91
SM-Reh/Y6	SVA CF	0.823	21.99	71.96	13.02
SM-CA-Reh/Y6	TA 80℃	0.843	20.73	53.84	9.41
SM-CA-Reh/Y6	TA 90℃	0.841	21.68	64.77	11.81
SM-CA-Reh/Y6	TA 100℃	0.836	22.93	77.38	14.83
SM-CA-Reh/Y6	TA 110℃	0.818	21.32	72.98	12.73
SM-Reh/Y6	TA 80℃	0.838	20.47	55.27	9.48
SM-Reh/Y6	TA 90℃	0.834	21.17	69.58	12.28
SM-Reh/Y6	TA 100℃	0.830	22.06	77.30	14.16
SM-Reh/Y6	TA 110℃	0.820	22.30	71.40	13.06

Table S10. Optimized device parameters of SM-CA-Reh/Y6 and SM-Reh/Y6 based devices. The average values and standard deviations were obtained from 6 devices, which were expressed as mean ± SD, n = 6

Active Layer	V_{OC} (V)	J_{SC}(mA/cm^2)	J_{SC}, cal (mA/cm^2)	FF (%)	PCE (%)
SM-CA-Reh/Y6	0.836 (0.834±0.009)	22.93 (22.17±0.44)	21.89	77.38 (75.80±1.56)	14.83 (14.01±0.36)
SM-Reh/Y6	0.830 (0.831±0.005)	22.06 (22.23±0.22)	21.05	77.30 (74.79±1.27)	14.16 (13.81±0.16)

Table S11. Devices parameters of OSCs based on SMDs reported by previous literatures.

Donor	Acceptor	V_{OC} (V)	J_{SC} (mA/cm^2)	FF (%)	PCE (%)	Ref.
BM-ClEH	BO-4Cl	0.846	24.38	72.7	15.0	3
BM-Cl	BO-4Cl	0.806	26.23	72.9	15.4	3
ZR2-C3	Y6	0.854	24.69	70.06	14.78	4
SW2	Y6	0.835	25.10	74.0	15.51	5
M-PhS	BTP-eC9	0.84	25.4	75.6	16.2	6
M-PhS-C2	BTP-eC9	0.873	26.62	72.38	17.11	7
BTR-Cl	Y6	0.85	23.9	65.1	13.81	8
BTR-Cl-C8	Y6	0.84	24.9	69.3	14.43	8
BTTzR	Y6	0.88	23.2	68.0	13.9	9
DAPor-DPP	6TIC	0.845	25.61	76.8	16.62	10
W2-CA	Y6	0.830	25.19	76.8	16.06	11
W2-Reh	Y6	0.826	25.31	74.8	15.63	11
HD-1	eOD	0.865	23.41	74.75	15.13	12
SM-CA	N3	0.838	24.33	75.62	15.41	1
SM-CA-Reh	N3	0.842	25.06	77.50	16.34	1
SM-Reh	N3	0.834	25.42	69.64	14.76	1
G-Dimer-D1	DY	0.858	23.47	70.06	14.12	13
G-Dimer-D2	DY	0.858	24.40	75.00	15.70	13
G-Dimer-D3	DY	0.859	24.36	76.64	16.05	13

Table S12. Properties and performance based on different monomers and linkers of dimeric donors.

Monomer	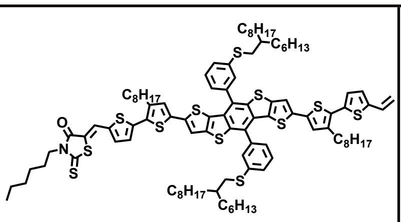		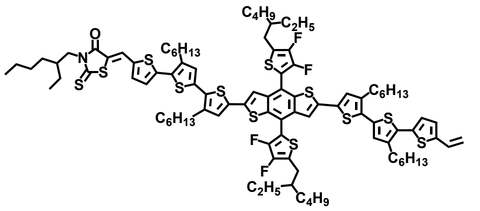		
Linkers	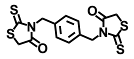 semi-flexible	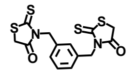 semi-flexible	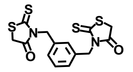 semi-flexible	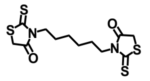 flexible	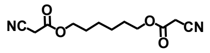 flexible
Positions	staircase	perpendicular	perpendicular	staircase	line
ΔG_{ls} (J/g)	-8.86	-5.72	-2.51	-1.40	-1.49
$\chi_{contact\ angle}$	0.44	0.52	0.17	0.26	0.34
HOMO (eV)	-5.39	-5.42	-5.32	-5.33	-5.31
FF (%)	/	75.14	71.56	68.87	65.21
J_{SC} (mA/cm^2)	/	24.11	27.39	26.34	23.13
V_{OC} (V)	/	0.844	0.800	0.794	0.758
E_{loss} (eV)	/	0.552	0.589	0.592	0.660

Table S13. Devices parameters of OSCs based on BDT-Dimer3/DY.

condition		V_{OC} **(V)**	**FF(%)**	J_{SC} **(mA/cm^2)**	**PCE (%)**
Donor concentration	8mg/mL	0.834	66.55	22.38	12.42
	9mg/mL	0.828	67.91	23.07	12.97
	10mg/mL	0.833	67.47	21.86	12.28
TA temperaure	130℃	0.853	69.15	22.89	13.50
	140℃	0.846	67.33	24.51	13.95
	150℃	0.813	69.56	23.82	13.47
DCBB concentration	10mg/mL	0.820	67.00	24.82	13.64
	11mg/mL	**0.832**	**69.48**	**24.63**	**14.24**
	12mg/mL	0.829	68.91	24.27	13.87

Supplementary Reference

1. J. Ge, L. Hong, H. Ma, Q. Ye, Y. Chen, L. Xie, W. Song, D. Li, Z. Chen, K. Yu, J. Zhang, Z. Wei, F. Huang and Z. Ge, *Adv. Mater.*, 2022, **34**, 2202752.
2. P. Virtanen, R. Gommers, T. E. Oliphant, M. Haberland, T. Reddy, D. Cournapeau, E. Burovski, P. Peterson, W. Weckesser, J. Bright, S. J. van der Walt, M. Brett, J. Wilson, K. J. Millman, N. Mayorov, A. R. J. Nelson, E. Jones, R. Kern, E. Larson, C. J. Carey, I. Polat, Y. Feng, E. W. Moore, J. VanderPlas, D. Laxalde, J. Perktold, R. Cimrman, I. Henriksen, E. A. Quintero, C. R. Harris, A. M. Archibald, A. H. Ribeiro, F. Pedregosa, P. van Mulbregt and C. SciPy, *Nat. Methods*, 2020, **17**, 261−272.
3. W. Gao, R. Ma, T. A. Dela Peña, C. Yan, H. Li, M. Li, J. Wu, P. Cheng, C. Zhong, Z. Wei, A. K. Y. Jen and G. Li, *Nat. Commun.*, 2024, **15**, 1946.
4. R. Zhou, Z. Jiang, Y. Shi, Q. Wu, C. Yang, J. Zhang, K. Lu and Z. Wei, *Adv. Funct. Mater.*, 2020, **30**, 2005426.
5. S. Wu, W. Feng, L. Meng, Z. Zhang, X. Si, Y. Chen, X. Wan, C. Li, Z. Yao and Y. Chen, *Nano Energy*, 2022, **103**, 107801.
6. L. Zhang, X. Zhu, D. Deng, Z. Wang, Z. Zhang, Y. Li, J. Zhang, K. Lv, L. Liu, X. Zhang, H. Zhou, H. Ade and Z. Wei, *Adv. Mater.*, 2021, **34**, 2106316.
7. L. Zhang, R. Sun, Z. Zhang, J. Zhang, Q. Zhu, W. Ma, J. Min, Z. Wei and D. Deng, *Adv. Mater.*, 2022, **34**, 2207020.
8. S. Ahmed, K. Yang, Y. Chen, H. Chen, P. Huang, S. Xue, Z. Xiao and S. Lu, *Dyes Pigments*, 2024, **228**, 112240.
9. Y. Wang, Y. Wang, L. Zhu, H. Liu, J. Fang, X. Guo, F. Liu, Z. Tang, M. Zhang and Y. Li, *Energy Environ. Sci.*, 2020, **13**, 1309−1317.
10. W. Zou, X. Zhang, H. Shen, W. Zhang, X. Jiang, L. Ni, C. Shen, L. Geng, X. Hao, Y. Yang, X. Wang, R. Yang, Y. Sun, Y. Kan and K. Gao, *SusMat*, 2024, **4**, e203.
11. Q. Wang, X. Zhang, Y. Miao, X. Jiang, X. Wang, Z. Zhang, Z. Lv, T. Liu, B. Zou, H. Xu, R. Yang, Y. Kan, Y. Sun and K. Gao, *ACS Mater. Lett.*, 2024, **6**, 713−719.
12. W. Feng, Y. Bai, J. Wang, S. Yuan, X. Wan, Y. Chen, B. Kan and Y. Chen, *Chin. J. Chem.*, 2024, **42**, 3075−3082.
13. C. Wang, X. Ma, D. Deng, H. Zhang, R. Sun, J. Zhang, L. Zhang, M. Wu, J. Min, Z.-G. Zhang and Z. Wei, *Nat. Commun.*, 2024, **15**, 8494.